



**NATIONAL UNIVERSITY OF SCIENCE AND
TECHNOLOGY
POLITEHNICA BUCHAREST**



DOCTORAL SCHOOL OF ELECTRICAL ENGINEERING

PhD Thesis Abstract

Numerical models for analyzing electrical machines with permanent magnets

PhD student:

Eng. Teodor-Ionuț ICHIM

Scientific supervisor:

Prof. Dr. Eng. Laurențiu-Marius Dumitran

**BUCHAREST
2025**

TABLE OF CONTENTS

1. INTRODUCTION	4
1.1. STUDY PURPOSE.....	4
1.2. PAPER CONTENT.....	5
2. GENERAL ELEMENTS OF HYBRID STEPPER MOTORS.....	6
2.1. STEPPER MOTOR CLASSIFICATION	7
2.1.1. <i>Variable reluctance stepper motors</i>	7
2.1.2. <i>Stepper motors with permanent magnets</i>	7
2.1.3. <i>Hybrid stepper motors</i>	7
3. NUMERICAL MODELING THE HSM	8
3.2 HYBRID NUMERICAL MODELS OF THE HSM	8
3.3 HSM THREE-DIMENSIONAL MODELING USING COMBINED A AND V_m FORMULATIONS.	9
3.3.1. <i>HSM numerical models using a combined A-V_m formulation</i>	9
3.4. CHOOSING THE TYPE OF FINITE ELEMENTS	10
3.5. METHODS FOR SOLVING LARGE MATRIX SYSTEMS.....	11
3.6. COMPARATIVE ANALYSIS OF ITERATIVE METHODS USED TO SOLVE LARGE MATRIX SYSTEMS	11
3.6.1. <i>Comparison between certain iterative solvers when different types of preconditioning are used</i>	11
3.6.2. <i>Convergence of the iterative FGMRES solver when different preconditioning methods are used</i>	12
3.6.4. <i>Convergence of iterative FGMRES and CG solvers for nonlinear systems</i>	13
4. NUMERICAL ANALYSIS OF AN HSM WITH SOLID MAGNETIC CIRCUIT	13
4.1. STUDY OF A BI-PHASE HSM USING THE SIMPLIFIED MODEL	14
4.1.1. <i>Analyzing the influence of the tooth width on the torque</i>	14
4.1.2. <i>Analyzing the influence of the permanent magnet height on the torque</i>	14
4.1.3. <i>Analyzing the influence of the distance between the rotor crowns on the torque</i>	15
4.1.4. <i>Optimizing the dynamic response of the engine</i>	15
4.1.5. <i>The detent torque</i>	15
4.1.6. <i>Analyzing the influence of the size of the air-gap on the torque</i>	15
4.1.7. <i>Holding torque vs. current characteristic</i>	16
4.2. OPTIMIZATION OF THE HSM WITH THE STATOR AND ROTOR MADE OF SOLID MATERIAL USING THE EXTENDED MODEL.....	16
4.2.1 <i>Details of the HSM extended model</i>	16
4.2.2. <i>Criteria used for the constructive optimization of HSM</i>	17
4.2.4. <i>The influence of the permanent magnet height on the holding torque</i>	17
4.2.5. <i>Changing the space between the rotor crowns</i>	18
4.2.6. <i>The influence of the stator pole shoe height on the holding torque</i>	18
4.2.8. <i>The influence of the stator yoke height on the holding torque</i>	19
4.2.9. <i>The comparison of the models studied</i>	19
4.3. HYBRID STEPPER MOTORS WITH MULTIPLE ROTOR STACKS AND DIFFERENT NUMBERS OF STATOR POLES..	20
4.3.1. <i>Influence of the number of rotor stacks on the holding torque</i>	20
4.3.1.1. <i>HSM with one rotor stack (single stack)</i>	20

4.3.1.3. HSM with three rotor stacks (triple stacks)	21
4.3.2. <i>HSM with different stator poles</i>	21
4.3.2.1. Comparison conditions of the studied design topologies	21
4.3.2.2. HSM with 12 poles and two rotor stacks.....	22
4.3.2.4. HSM with 24 poles and two rotor stacks.....	23
4.3.2.5. HSM with 40 poles and two rotor stacks.....	24
5. ANALYSIS OF AN ANISOTROPIC HSM WITH A LAMINATED STATOR AND SOLID ROTOR USING THE EXTENDED MODEL	25
5.1. INFLUENCE OF THE LAMINATION STACKING FACTOR ON THE HOLDING TORQUE	25
5.1. INFLUENCE OF THE AIR GAP HEIGHT ON THE HOLDING TORQUE	26
5.2. COMPARISON BETWEEN ISOTROPIC (SOLID STATOR) AND ANISOTROPIC (LAMINATED STATOR) MODELS OF THE HSM	26
5.3. OPTIMIZATION OF THE HSM WITH LAMINATED STATOR	27
6. ANALYSIS OF THE DETENT TORQUE OF THE HSM	28
6.1. 3D NUMERICAL MODEL OF THE HYBRID STEPPER MOTOR FORMULATED WITH MAGNETIC VECTOR POTENTIAL A	29
6.2. 3D NUMERICAL MODEL OF THE HYBRID STEPPER MOTOR FORMULATED WITH MAGNETIC SCALAR POTENTIAL V_M	29
6.3. COMPARISON BETWEEN THE NUMERICAL MODEL DEFINED WITH MAGNETIC VECTOR POTENTIAL A AND THAT DEFINED WITH MAGNETIC SCALAR POTENTIAL V_M	30
6.4. COMPARISON BETWEEN THE DETENT TORQUE OF THE HSM WITH LAMINATED STATOR AND THAT WITH SOLID STATOR	30
7. MANUFACTURING AND TESTING A BI-PHASE HSM PROTOTYPE WITH LAMINATED STATOR	31
7.1. HSM PROTOTYPE	31
7.3. VALIDATION OF THE STUDIED TWO-PHASE HSM.....	32
7.3.1. <i>Test bench of HSM</i>	32
7.3.2. <i>Measuring the detent torque</i>	32
7.3.2.1. Measurement of the friction torque.....	32
7.3.2.2. The measurement of the HSM total torque in the absence of current	33
7.3.2.3. Determination of detent torque.....	33
7.3.3. <i>Measuring the HSAM static torque</i>	34
7.3.4. <i>Comparison between numerical and experimental results</i>	35
7.3.4.1. Detent torque	35
7.3.4.2. Holding torque	35
8. FINAL REMARKS	35
8.1 RESULTS ACHIEVED.....	35
8.2 AUTHOR'S ORIGINAL CONTRIBUTIONS	36
8.3 PUBLISHED PAPERS	38
8.4 PERSPECTIVES FOR FURTHER DEVELOPMENT	39
9. SELECTED REFERENCES	41

1. INTRODUCTION

Since their discovery, electric machines have undergone continuous evolution, becoming vital in various industrial and commercial applications. A major contributor to this progress has been the development and growing use of permanent magnets. Additionally, the integration of microcontrollers has enhanced the management of the motors' operations, resulting in significantly improved efficiency and precision.

The comprehensive understanding of electric motor operations and their design as an integrated system, along with the drive system, has led to increased diversification and development in the electric vehicle market. As a result, high-power electric motors used in electric traction, as well as high-power electric generators, have now been built using permanent magnets, a solution previously feasible only for low-power machines. Additionally, smaller machines, used as transducers or actuators, have become increasingly precise and compact due to advancements in materials and manufacturing methods. It is worth noting that among all electric machines, only the induction machine cannot be built using permanent magnets.

1.1. STUDY PURPOSE

Electric machines with a common design have axial symmetry. This allows the usage of two-dimensional FEM numerical models for computing the electromagnetic field distribution in the machine's cross-section. Among the electric machines, the most complex are those with axial field distribution, such as claw-pole synchronous machines and stepper hybrid motors. Since these machines lack symmetry in their magnetic field distributions, as they have both transverse and axial components, numerical analysis must be conducted using three-dimensional models.

The author selected a two-phase hybrid stepper motor (HSM) as the case study due to its complexity and the challenges associated with modeling and optimizing this type of motor. The findings from this doctoral research, along with the insights presented in this work, are not only significant for this type of motor but also for the numerical modeling and optimization of electric machines in general. A prototype of the HSM, which served as the foundation for this doctoral study, was created and experimentally tested at ICPE S.A. in the MESSICO department.

Traditionally, the MPP design has been achieved using empirical knowledge and analytical calculations, and two-dimensional numerical models to analyze the air-gap area and the motor tooth region [1-3]. Another factor that increases model complexity and the motor's numerical optimization is the magnetic anisotropy of the magnetic circuits made of laminations [4].

Another aspect studied was the calculation and measurement of the detent torque and parasitic torques of a hybrid MPP. These low-value torques are difficult to calculate using numerical modeling, but they are important for fine mechanisms, such as those used in space applications.

1.2. PAPER CONTENT

In the first part of this paper, the author presents as comprehensively as possible the general aspects regarding the construction, control, and applications of the HSM. More detailed explanations are provided for the two-phase HSM, the type of motor studied in the paper.

In the next chapter, the author presents important aspects regarding numerical modeling using Finite Element Method (FEM). Several previous scientific works focused on reducing computational time, such as hybrid models using equivalent magnetic circuits or virtual magnetic flux barriers coupled with two-dimensional magnetic field FEM model, to account for the axial magnetic flux [3,5-8].

In the next chapter, a comparison of different solvers used to compute large linear equation systems, regarding their efficiency and computer memory consumption, is presented. Several iterative solving methods coupled with different preconditioning algorithms are analyzed.

Then, models based on combining the magnetic scalar potential V_m domains with those defined with the magnetic vector potential \mathbf{A} were analyzed. Between the domains defined with different potentials, a continuity condition was imposed. Once the most appropriate methods of solving and the most advantageous potential formulations have been established, the author develops four different models of the studied HSM:

1. A three-dimensional isotropic HSM model, called the *simplified model*, neglecting the leakage magnetic field, using a mixed formulation based on both scalar and vector magnetic potentials, and having a sliding surface at the air-gap level to allow simulating the rotor movement without reconstructing the finite element mesh.
2. An air domain surrounding the motor was added to the first model, as well as the geometry of the end windings to account for the magnetic leakage field and fringing effect. This model is called *the extended model*.
3. The previous three-dimensional model, considering the magnetic leakage field, was modified to study the HSM with the stator made of laminations. The stator iron is magnetic anisotropic, as the magnetic permeability along the axial direction is greatly reduced compared to the values for the other two directions. This model has been called *the anisotropic extended model*.
4. The fourth model has a high resolution, having a very large number of finite elements. It is based on either the scalar magnetic potential or the vector potential. The model was used to compute the detent torque of the HSM.

Compared to similar works analyzing the impact of the tooth shape on the HSM holding torque [10-15], this paper presents a more detailed analysis in which several other constructive geometric parameters are taken into account. These are the permanent magnet radial and axial dimensions, the pole width, the shoe pole width, the stator yoke height, etc. The influence of the airgap size on the torque developed by the motor is also studied. In addition, a reduction of the detent torque by modifying the stator tooth pitch against the rotor tooth pitch is presented.

Using *the isotropic extended model*, an analysis of different constructive topologies of the HSM with the stator made of solid material was performed. The holding torque of an HSM with different poles/slots in the stator was calculated. Consequently, an algorithm was developed and used for calculating the pole positions to achieve a correct alignment of the stator teeth with the teeth in the rotor. The influence of the number of rotor stacks on the HSM holding torque was also analyzed, preserving the geometric envelope of the original motor.

The anisotropic extended model was used to analyze a two-phase HSM with the stator made of laminations. The influence of the stacking factor on the motor holding torque was studied. The anisotropic HSM was then optimized, resulting in an increase of almost 30% in the torque compared to the initial motor.

Another aspect studied was the determination of the detent torque from numerical modeling. The detent torque was computed using three-dimensional FEM models with subsequently refined discretization meshes, generating tens of millions of unknowns.

In the final part, the author validates the FEM numerical analysis of an anisotropic HSM, by comparing the numerical results with the experimentally measured data. The author presents conclusions regarding the experimental measurements of the detent and parasitic torques measured on the test bench, torques with very small values, but important for motors used in refined, precision mechanisms.

2. GENERAL ELEMENTS OF HYBRID STEPPER MOTORS

Stepper motors (SM) are synchronous machines with variable reluctance. There are three constructive types of SMs: variable reluctance SM, permanent magnet SM, and HSM. All of these have in common that the rotor moves in discrete steps of equal size, which is why they are called stepper motors [16]. The reluctance torque period of the variable reluctance SM is twice the period of the shaft torque. This allows variable SM to achieve higher speeds compared to HSM, which has a reluctance torque period that is only one-fourth of the electromagnetic torque period. Additionally, the permanent magnets placed in the rotor of the HSM provide stronger magnetic coupling, which results in higher torques.

From the constructive perspective, the HSM is a combination of the two variants of SM, which is why it is called a *hybrid motor*. In its common construction, the HSM has both permanent magnets and teeth/poles that generate variable reluctance in operation. Compared to the other two variants, the HSM has many teeth, and like the claw-pole synchronous machine, the number of teeth on one rotor crown equals the number of pole pairs. Due to its reduced travel step, the HSM is preferred in applications where positioning accuracy is critical [17] and/or when high torques at low speed are required [18].

Due to their constructive diversity, SMs can produce shaft torques in a wide range, starting from around 1 μ Nm (in tiny motors with external diameters of up to 3mm), up to 40 Nm (in industrial applications, mainly for machine tools), with diameters of up to 150 mm, [19]. Also, SMs with variable reluctance can easily reach speeds of 20,000 steps/s. In contrast, using a micro-stepping technique, HSMs can achieve travel steps of only 0.036° [20].

2.1. STEPPER MOTOR CLASSIFICATION

2.1.1. Variable reluctance stepper motors

From the construction perspective, variable reluctance SMs can be classified into: single-rotor variable reluctance SMs and variable reluctance SMs with multiple rotors.

SMs with variable reluctance and a single rotor usually have pole pitch angles ranging from a few degrees to 45° and speeds between 1000 and 20,000 steps/s [22,23]. A multi-rotor variable reluctance SM is built with several rotors mounted on the same shaft, each having the same number of teeth, thus the same pole pitch.

Variable reluctance SMs have the advantage of a robust construction, as they do not have permanent magnets or windings in the rotor. They have a reduced moment of inertia compared to machines with windings in the rotor, and because they have a larger pole pitch than the HSMs, they can operate at much higher speeds. SMs with variable reluctance and multiple rotors can be built with up to seven rotors and therefore have seven phases. Usually, these motors have an angular pitch between 2° and 15° .

2.1.2. Stepper motors with permanent magnets

Permanent magnet SMs are synchronous motors that, in their classical construction, have several pole pairs p made of permanent magnets with alternating polarity embedded in the rotor. In the stator, they have a winding with m phases and the same number of pairs of poles p as in the rotor. Due to their permanent magnets, these types of SMs have higher cogging torques compared to variable reluctance SMs that have zero cogging torque. Permanent magnet SMs can be constructed with a large number of pole pairs when a small moving step, i.e., high resolution of motion, is required [27, 28].

2.1.3. Hybrid stepper motors

HSM is a combination of the first two types of SM, the variable reluctance SM and the permanent magnet SM. That is why, in addition to an electromagnetic torque, it also generates a variable reluctance torque produced by the relative position between the stator and the rotor teeth. These motors are especially used as actuators where factors such as resolution, sensitivity, and accuracy of the angular positioning are essential.



Figure 2.1 HSM parts: a) stator, b) rotor assembly [32, 33].

Variable reluctance SM is the motor that can develop the highest speeds among stepper motors, while permanent magnet SM produces average torques and speeds. HSM has the highest torque density and motion resolution. The properties comparison of the three stepper motor variants is shown in Table 2.1 [36].

Table 2.1 Comparison between the three types of SMs.

Advantages / Types of SM	MPP with variable reluctance	MPP with permanent magnets	MPP Hybrid
Angular step	<1.8°	>7.5°	<1.8°
Active torque	Small	Moderate	High
Reluctance torque	Small	Sea	Moderate
Pulse Rate/Speed	Sea	Small	High
Acceleration/response	Fast	Slow	Fast
Noise	Noisy	Low noise	Low noise
Micro stepping	Not	Yes	Yes
Design	Moderate	Simple	Complex

3. NUMERICAL MODELING THE HSM

Modeling HSM is complex due to the distribution of the magnetic field, which has two components. One type of magnetic field is transversal, produced by the stator windings, while the other is axial, generated by the ring-shaped magnet or magnets located in the rotor. Modeling the hybrid MPP is also complicated due to the motor's rotor, which has many tiny teeth, and a very small air gap compared to other electric machines. That is why the only solution to accurately design such motors is to use three-dimensional numerical modeling of the magnetic field distribution inside the HSM. Due to the small size of the air gap, three-dimensional Finite Element Method (FEM) models produce very large systems of equations that are impractical to solve using direct methods. This has contributed to a scarcity of research on the HSM in recent years. To address the limitations of available computing power at the time, many authors proposed hybrid models that combined analytical calculations with simplified two-dimensional numerical models.

3.2 HYBRID NUMERICAL MODELS OF THE HSM

Due to its difficult design, many HSMs are made using a kind of template, based on the NEMA standard, where the motor's main geometric parameters are imposed. This approach is also facilitated by the modular structure of the HSM, which can be built with multiple rotor stacks to obtain a proportionally higher torque.

An alternative to three-dimensional numerical modeling, which consumes a lot of time and computational memory, a prohibitive approach until recently, has been the hybrid models. They are based on two-dimensional FEM numerical models coupled with analytical calculations. Although these hybrid models significantly reduce the computational time, they are approximate and do not achieve the accuracy of a complete, three-dimensional model based on

the real, spatial geometry of the motor. Lately, there have been papers presenting results of the HSM three-dimensional modeling [34,52], with declared errors of around 5% compared to the experimental measurements.

3.3 HSM THREE-DIMENSIONAL MODELING USING COMBINED \mathbf{A} AND V_m FORMULATIONS.

Using COMSOL's *Rotating Machinery, Magnetic* module, both magnetic vector potential \mathbf{A} and the scalar potential V_m can be used. The COMSOL documentation recommends that, for electric machines with permanent magnets, the "stitching" surface between the rotor domain, which is defined with the scalar potential, and the stator domain, which is defined with the vector potential, should be located in the air-gap. As shown in this chapter, the computational domain can be divided in a much more diverse way among the subdomains defined with the two potentials.

3.3.1. HSM numerical models using a combined \mathbf{A} - V_m formulation

To study the reduction of the computational time by combining domains defined with the magnetic vector potential \mathbf{A} with domains defined with the scalar potential V_m , three-dimensional models of an HSM with a moving step of 0.3° were developed. The motor has 300 teeth, making it one of the motors with the smallest angular step on the market. By comparison, HSMs presented in research papers such as [57-59] or those marketed by manufacturers such as Sagem, Sener, or Phytron [61-63] have an angular step of 1° , 1.8° , or 3.6° . Indeed, some manufacturers are producing "alpha" series of HSM, which are motors customized according to the beneficiary's needs. But these motors are expensive, as the high costs of research and prototyping must be covered.

The studied bi-phase HSM has 48 slots/poles in the stator, which is a special construction that differs from the common solutions with eight poles. This motor was chosen because of its physical symmetry, which allowed the reduction of the computational domain to $1/12^{\text{th}}$ of the motor geometry.

Variants A, B, C, D, and E of the numerical models of the studied HSM

Five models of the studied motor were developed, using a different combination of the subdomains defined with the vector and scalar magnetic potentials.

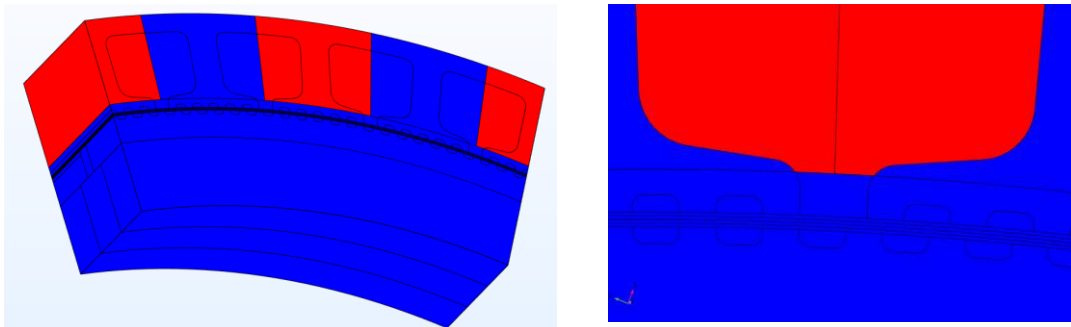


Figure 3.1 3D computing domain of the magnetic field problem – Variant C: red – the subdomains defined with the magnetic potential vector \mathbf{A} , blue – the subdomains defined with the scalar magnetic potential V_m .

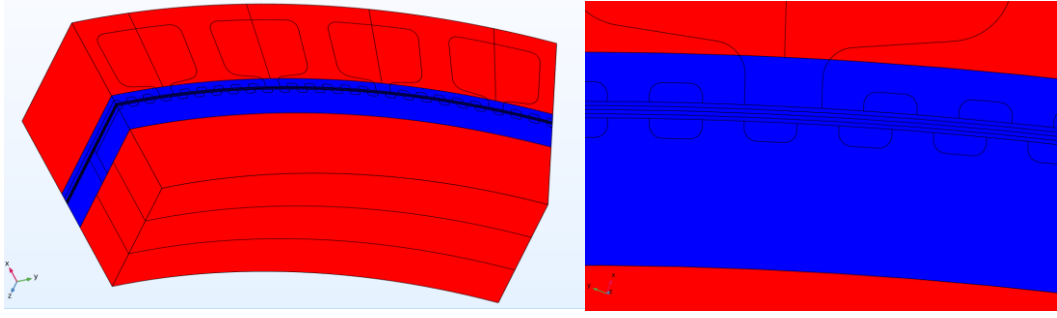


Figure 3.2 The definition of the 3D magnetic field problem – Variant E: red – the subdomains defined with the magnetic potential vector \mathbf{A} , blue – the subdomains defined with the scalar magnetic potential V_m .

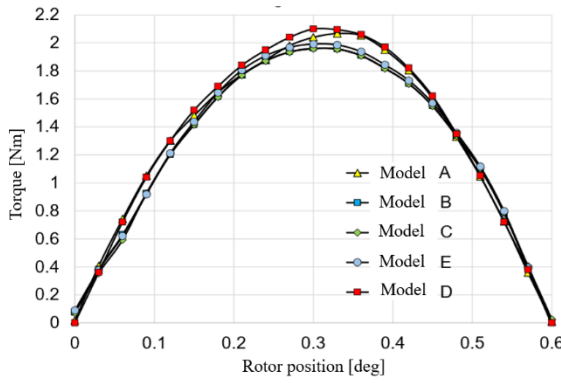


Figure 3.3 Comparison of the torque characteristic computed using Models A, B, C, D, and E.

A comparison of the HSM static mechanical characteristics determined using all the above models is shown in Figure 3.10. The geometry, the discretization mesh, and the solver used were the same. To solve these field problems, a computer with an i5-12600K CPU and 64 GB of RAM was used. The torque was computed using relation (3.12). Table 3.1 shows that *Model D*, which is based only on the magnetic potential vector \mathbf{A} formulation, is impractical, as the solution took about 20h.

Table 3.1 Calculation time and error using the five different HSM numerical models.

	Model D	Model A	Model B	Model C	Model E
Computing time	Approx. 20h	1h 40'	1h	40'	1h
Error	Reference model	1%	4.3%	4.4%	3%

3.4. CHOOSING THE TYPE OF FINITE ELEMENTS

In the process of modeling with the help of MEF, the following three aspects are of the greatest importance: the choice of unknown potentials for the formulation of the problem, as shown above, the way of discretizing the domain in finite elements and the method of solving the resulting system of equations. These aspects influence the time and memory required to obtain the solution, as well as its accuracy.

In the case of three-dimensional MEF modeling, it is possible to use tetrahedron, triangular prism or parallelepiped elements. In addition, the elements can be of the first order, or of the higher order, depending on the order of the interpolation functions. As a general rule, in order to obtain more accurate results, it is preferable to use first-order elements and to use them in areas of intense field or with high gradient, instead of higher-order elements. This strategy was also used in this case.

3.5. METHODS FOR SOLVING LARGE MATRIX SYSTEMS

Solving systems of equations with a large number of unknowns can be achieved using a variety of solvers. The chosen method depends on the coefficient matrix (the Jacobian), which can be symmetrical or non-symmetrical, positive defined or not, sparsely or densely populated, or otherwise. In many FEM models, the resulting coefficient matrix is symmetric and positive, and sparse. These solving methods can be direct when an exact solution is achieved after a given, known number of successive computations, and iterative, when a series of successive approximations of the solution that converge to the exact solution are generated.

Compared to direct solvers, iterative solvers have the advantage that they can use the solution from the previous non-linear iteration (or time step) as an approximate solution for the current iteration to identify the desired solution more quickly. In general, the number of computations that an iterative algorithm performs is significantly lower than that used by a direct solver. Usually, an accurate enough solution can be achieved using an iterative solver with many fewer iterations than would be required for obtaining the exact solution [64].

3.6. COMPARATIVE ANALYSIS OF ITERATIVE METHODS USED TO SOLVE LARGE MATRIX SYSTEMS

Several of the well-known iterative methods used for solving linear systems are analyzed concerning their convergence speed and computer memory requirements.

The methods analyzed are: FGMRES (Flexible generalized minimum residual), CG (Conjugate gradient), BiCGStab (Biconjugate Gradient Stabilized), TFQMR (Transpose-free quasi-minimal residual).

3.6.1. Comparison between certain iterative solvers when different types of preconditioning are used

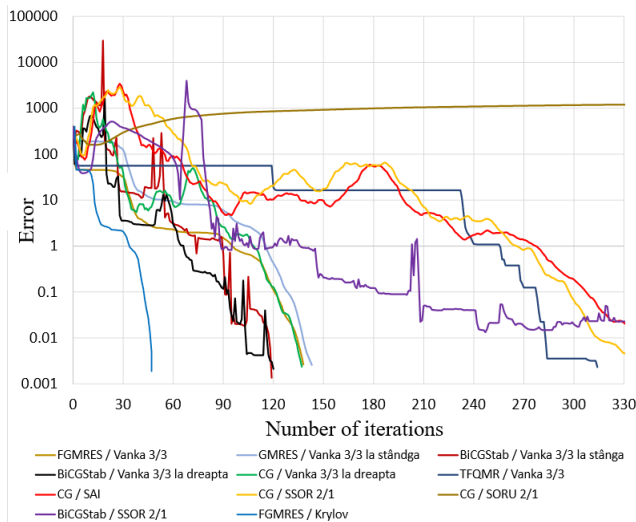


Figure 3.4 Error variation vs. iterations using FGMRES, GMRES, BiCGStab, CG, and TQMR solvers, and Vanka, SAI, SSOR, and SORU preconditioners.

The iterative methods studied have a convergence that can be improved depending on the preconditioning algorithm. As the preconditioning matrix approximates the inverse matrix of the system to be solved, the more accurate this approximation is, the faster the iterative solver converges. On the other hand, computing the preconditioning matrix with greater precision requires more time and computer memory. Thus, from one point onwards, it is no longer worth the effort.

3.6.2. Convergence of the iterative FGMRES solver when different preconditioning methods are used

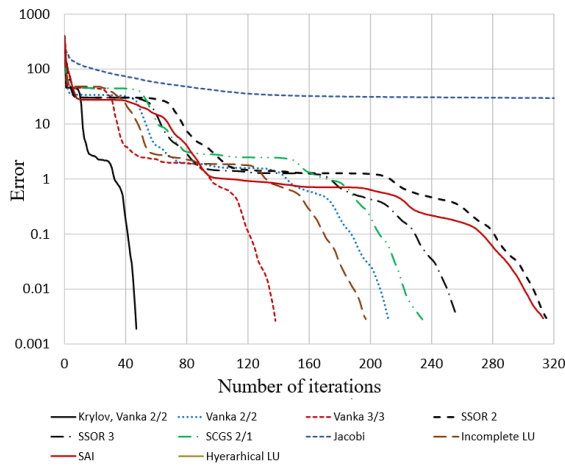


Figure 3.5 Error evolution when using FGMRES and different preconditioning methods.

One of the most efficient and stable solving methods (which converges towards the desired solution even for poorly numerically conditioned Jacobian matrices) is FGMRES, which will be studied further. As shown in Figure 3.19, the number of iterations and the speed of convergence of the method depend on the type of preconditioning used.

3.6.3. Convergence of the FGMRES and CG solvers

The following two fastest iterative solvers were analyzed: the Conjugate Gradient and FGMRES. They were used to

solve a FEM modeled magnetic field inside a HSM during idle operation.

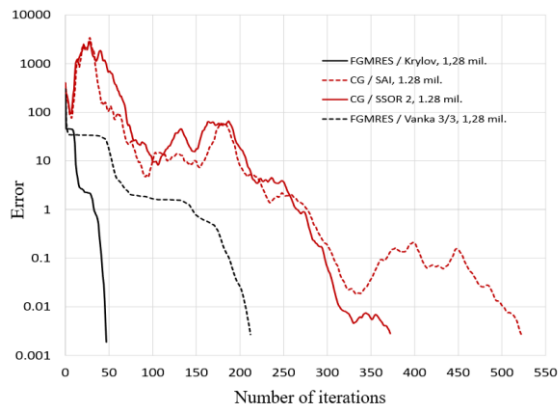


Figure 3.6 Error evolution when using FGMRES and CG solvers, and Krylov, Vanka, SSOR, and SAI preconditioners to solve a system with 1.287.192 unknowns.

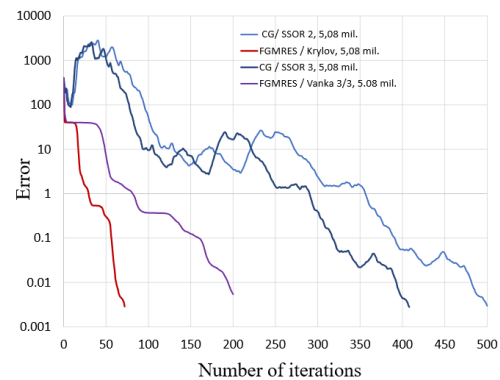


Figure 3.7 Error evolution when using FGMRES and CG solvers, and Krylov, Vanka, SSOR, and SAI preconditioning to solve a system with 1.287.192 unknowns.

The FGMRES solver becomes more efficient than gradient methods as the number of unknowns increases. Also, when solving nonsymmetric systems, the CG solver cannot be used and must be replaced by BiCGStab, which takes about twice as long to solve the linear system.

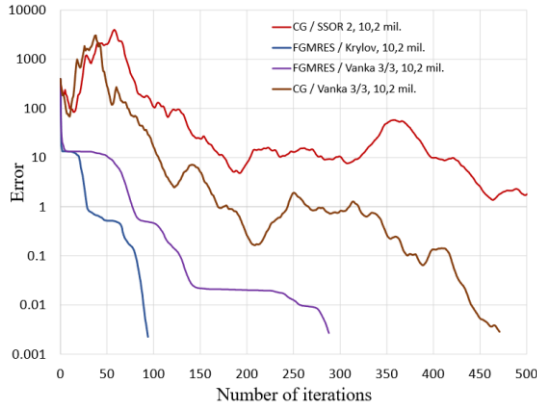


Figure 3.8 Error evolution when using FGMRES and CG solvers, and Krylov, Vanka, and SSOR preconditioning to solve a system with 10.254.636 unknowns.

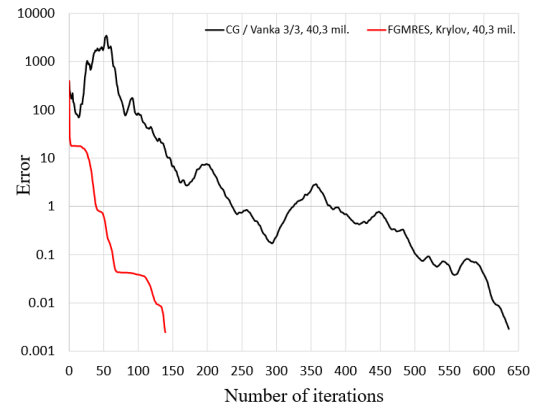


Figure 3.9 Error evolution when using FGMRES and CG solvers, and Krylov and Vanka preconditioning to solve a system with 40.322.361 unknowns.

3.6.4. Convergence of iterative FGMRES and CG solvers for nonlinear systems

For this analysis, a nonlinear numerical model having about 10 million unknowns was solved. The Newton-Raphson algorithm was used to solve the nonlinearity [73] in conjunction with two iterative solvers, FGMRES and CG. As shown in Table 3.9, the FGMRES iterations are noticeably fewer than those of CG. The FGMRES solver is more efficient when the iteration starts from an initial solution that is closer to the real solution.

The HSM nonlinear FEM models shown in this paper, were solved using a FGMRES solver with Krylov preconditioning, as this was proven to be the most time and memory efficient.

Table 3.2 Computation time and number of iterations when using FGMRES and the Conjugate Gradient solvers, and Newton-Raphson iterations.

Method	No. of unknowns	No. of iterations	Time [s]
FGMRES / Krylov	9.659.093	655	3059 (50min, 59s)
CG / SSOR 2	10.254.636	8450	5815 (1h 36min 55s)

4. NUMERICAL ANALYSIS OF AN HSM WITH SOLID MAGNETIC CIRCUIT

Numerous research papers comprise analyses of the HSM tooth geometry, as their shape and width have an important impact on the motor torque [6, 13, 59, 75, 76]. Equally important geometric parameters, such as the permanent magnet shape and volume, the air-gap diameter, the yoke width, etc., are neglected in these studies.

To study the influence of these geometrical parameters on the torque produced by the HSM, FEM 3D numerical models were developed. An initial study was conducted using *the simplified model*. Subsequently, using the *homogeneous extended numerical model*, which accounts for the magnetic leakage flux and the geometry of the end windings, the number of stator slots/poles and the number of rotor packages were modified. The motor holding torque was computed,

maintaining the HSM geometric envelope, the resistance of the stator winding, and the supply voltage.

4.1. STUDY OF A BI-PHASE HSM USING THE SIMPLIFIED MODEL

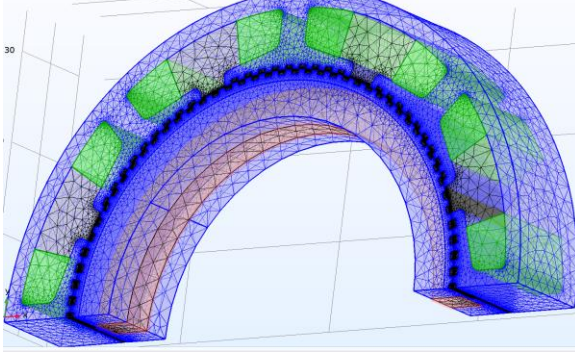


Figure 4.1 The HSM – computation domain discretization: coils (green), magnetic circuit (blue), permanent magnet (red).

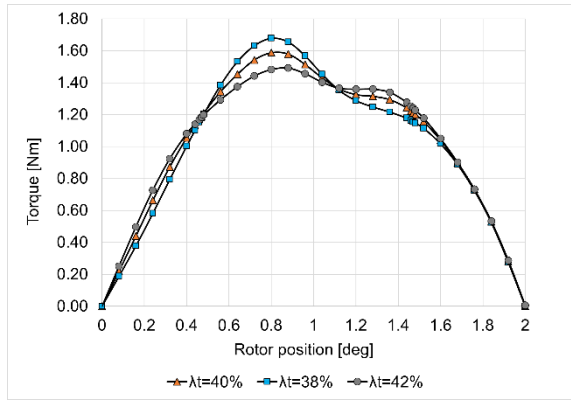


Figure 4.2 Torque static characteristics for different tooth widths.

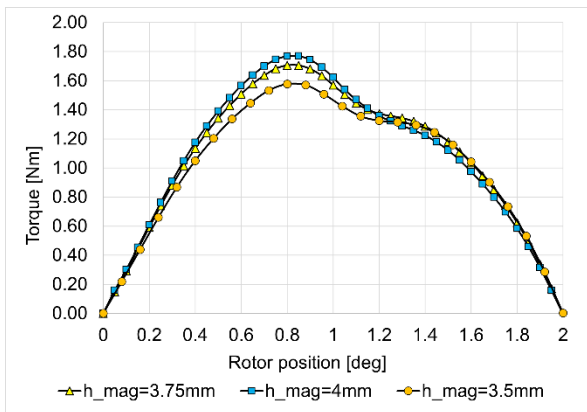


Figure 4.3 Torque static characteristics for different permanent magnet heights.

To simulate the rotor movement, consecutive stationary magnetic field problems were solved, one for each step of rotor position, using a slip band between the stator and the rotor. One of the two stator windings was supplied with a constant current density \mathbf{J} , while the rotor was rotated half of the electric period, equivalent to two degrees.

4.1.1. Analyzing the influence of the tooth width on the torque

The curves shown in Figure 4.4 are obtained for different λ_t ratios between the tooth width and the tooth pitch, chosen following the research recommendations [57, 79]. As shown in Figure 4.4, the higher holding torque values correspond to lower values of λ_t .

4.1.2. Analyzing the influence of the permanent magnet height on the torque

In the next study the radial size of the permanent magnet was changed. As shown in Figure 4.6, the holding torque increased from 1.6 Nm to 1.8 Nm as the permanent magnet height changed from $h_{mag} = 3.75 \text{ mm}$ to $h_{mag} = 4 \text{ mm}$.

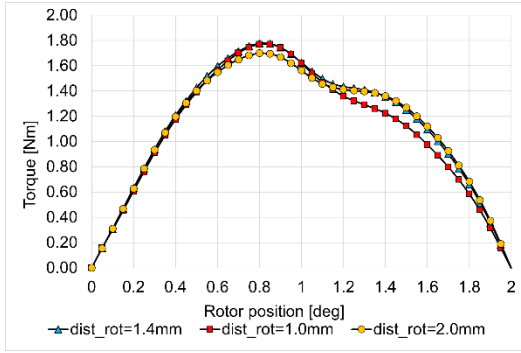


Figure 4.4 Torque variation depending on the rotor position for different distances between the crowns at the level of the interchange.

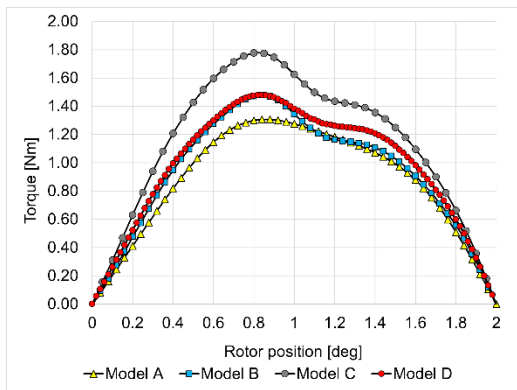


Figure 4.5 Static torque characteristic of MPP for the four models.

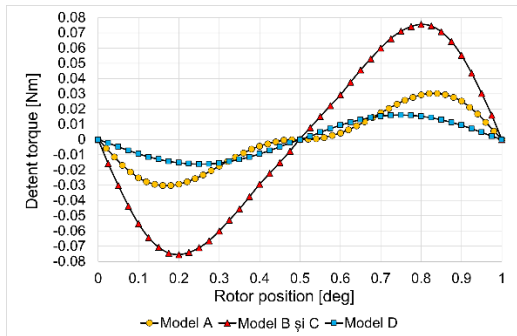


Figure 4.6 Detent torque for the four models presented above.

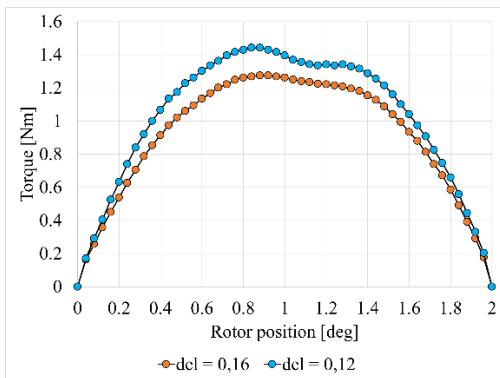


Figure 4.7 Static torque characteristic for 0.12 mm and 0.16 mm airgap size.

4.1.3. Analyzing the influence of the distance between the rotor crowns on the torque

The following analysis was done by reducing the space between the two rotor crowns from $dist_rot = 2$ mm to 1.0 mm. For $dist_rot = 1.4$ mm, the holding torque was $T_m = 1.8$ Nm, as shown in Figure 4.7.

4.1.4. Optimizing the dynamic response of the engine

All the models presented above were computed using the same 105 A-turns per coil (respectively 220 turns per coil) and the same geometric envelope. For the next study, four other motor variants, with different geometric parameters and ampere-turns, were compared.

4.1.5. The detent torque

Reducing the cogging torque (also called detent torque) can be achieved by a small alteration of the stator tooth pitch compared to the rotor tooth pitch. A tiny increase of the stator tooth pitch from 4° to 4.05° , *Model C* in Figure 4.10, diminished the detent torque to $1/4^{\text{th}}$ of its initial value.

4.1.6. Analyzing the influence of the size of the air-gap on the torque

Figure 4.11 shows the static mechanical characteristic of an identical HSM to the reference motor, apart from the airgap which was increased from 0.12 mm to 0.16 mm. The 33% increase of the airgap produced a reduction of the holding torque of about 14%.

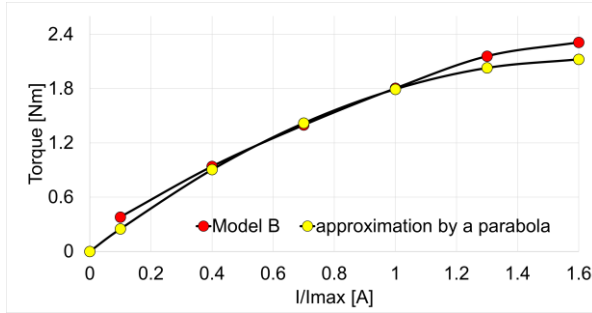


Figure 4.8 Holding torque vs. current dependence of the optimized HSM, *Model B*.

4.1.7. Holding torque vs. current characteristic

Figure 4.12 shows the holding torque as a function of the current in the stator winding, for the optimized HSM, *Model B*. The curve shows the degree of magnetic saturation of the HSM as the current is increased.

4.2. OPTIMIZATION OF THE HSM WITH THE STATOR AND ROTOR MADE OF SOLID MATERIAL USING THE EXTENDED MODEL

A geometric optimization of the bi-phase HSM with 1° step, also studied in paragraph 4.1, is performed using the *homogeneous extended model*, and presented below. The current and voltage have been kept unchanged.

4.2.1 Details of the HSM extended model

The model used for the following study had the "sewing" surface between the rotor and stator domains removed. As the continuity condition between the magnetic scalar potentials on the rotor and stator sides of the connecting boundary was eliminated, the iterative solver convergence increased. That produced a 30% reduction of the computational time for one rotor position, compared to previous model having the "sewing" surface, as shown in Table 4.3.

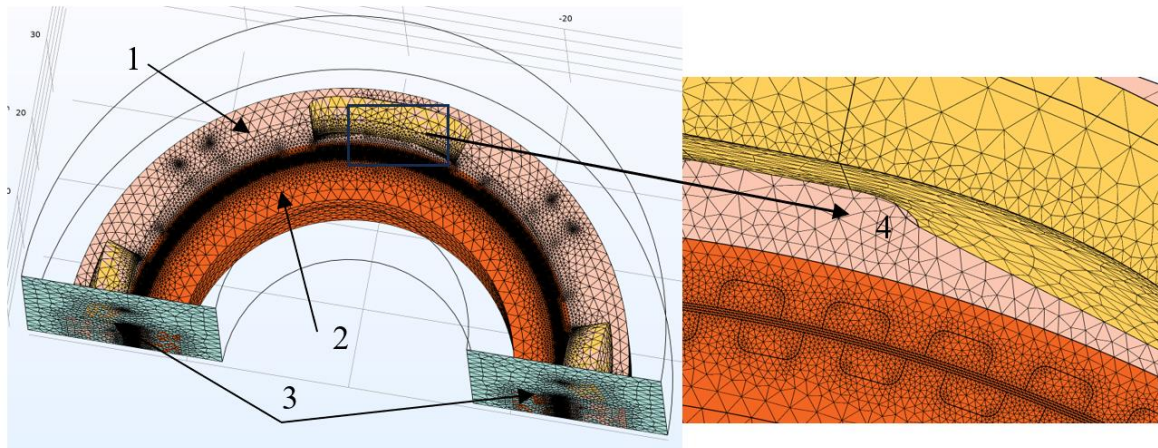


Figure 4.9 HSM – discretization of the computational domain: 1 – vector potential domain A , 2 – scalar magnetic potential domain V_m , 3 – periodicity conditions, 4 – airgap mesh detail.

Table 4.3 Computing time for the model with and without the sewing surface in the airgap using a PC with AMD Ryzen 5 3600 processor and 64 GB of DDR4 RAM.

Calculation for a single rotor position	Computing time	Number of unknowns
with the sewing surface	2h 10'	7,101,418
without the sewing surface	40'	3,981,001

4.2.2. Criteria used for the constructive optimization of HSM

The main goal of the HSM optimization was to obtain the highest holding torque possible. In addition, a lower electrical time constant was preferred. The study was carried out maintaining the phase current, the phase resistance, and the motor's geometric envelope constant. The air-gap was 0.15 mm.

4.2.4. The influence of the permanent magnet height on the holding torque

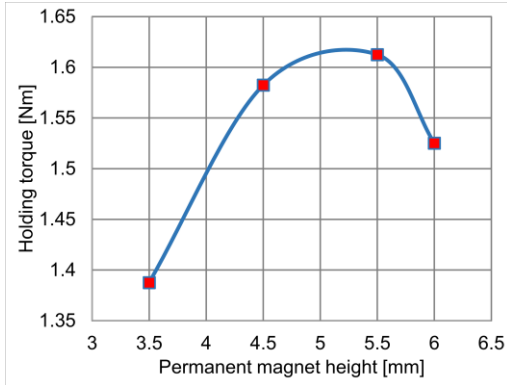
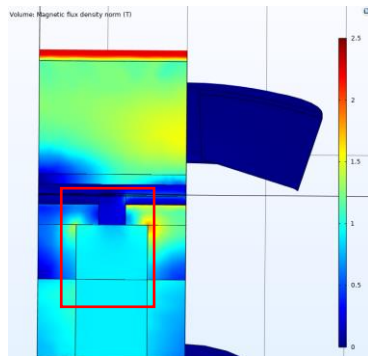
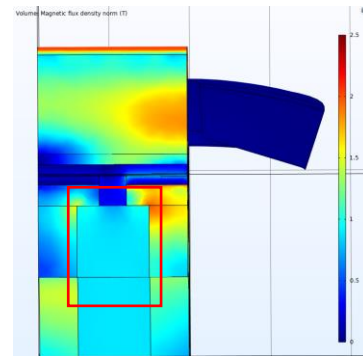


Figure 4.10 Holding torque vs. the permanent magnet height.

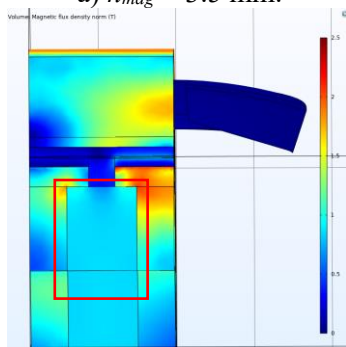
The second constructive analysis was conducted by modifying the height of the permanent magnet. As the rotor diameter has increased along with the magnet height, the slot area has decreased. Also, the number of coil turns has been adjusted to keep the phase resistance constant.



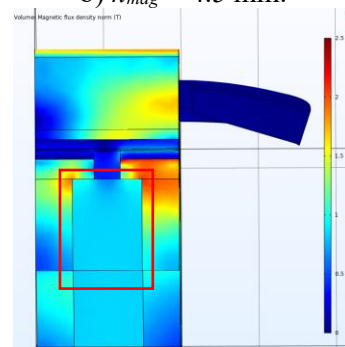
a) $h_{mag} = 3.5$ mm.



b) $h_{mag} = 4.5$ mm.



c) $h_{mag} = 5.5$ mm.



d) $h_{mag} = 6$ mm.

Figure 4.11 The distribution of the magnetic flux density for four permanent magnet heights.

4.2.5. Changing the space between the rotor crowns

The next study analyzed the modification of the distance between the rotor crown, respectively, the decrease of the geometric parameter called l_{umar} , Figure 4.20.

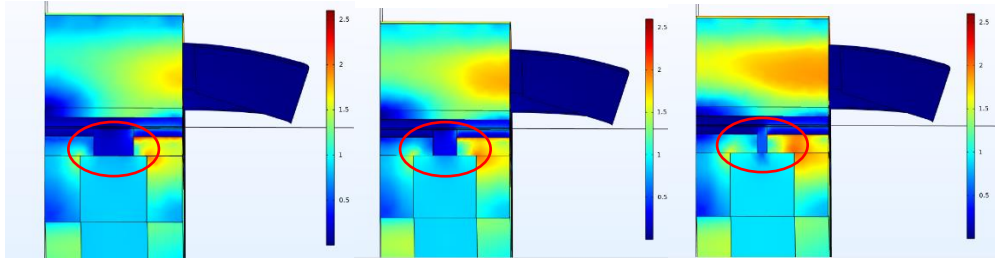


Figure 4.12 Magnetic flux density distribution map for three air gaps between the rotor crowns: left – $l_{umar} = 4.3$ mm; middle – $l_{umar} = 3.8$ mm; right – $l_{umar} = 3.3$ mm.

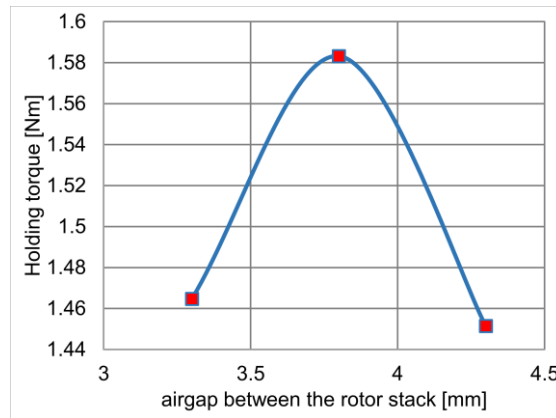


Figure 4.13 The holding torque versus airgap between rotor crowns.

4.2.6. The influence of the stator pole shoe height on the holding torque

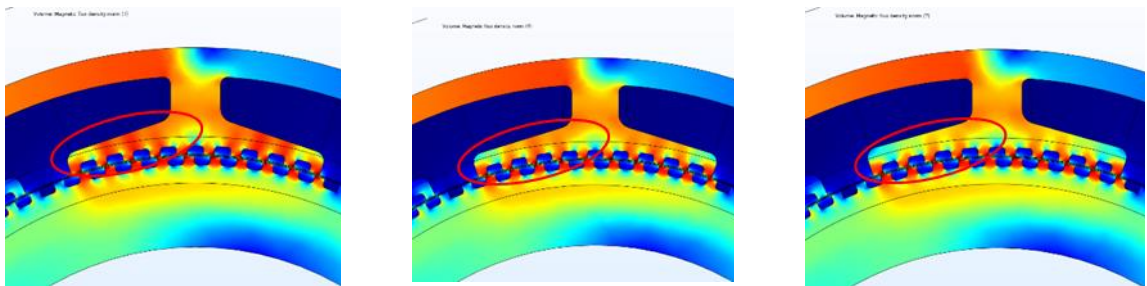


Figure 4.14 Magnetic flux density distribution for three different pole shoe heights: Left – $h_{talpă} = 1,5$ mm; Middle – $h_{talpă} = 1,7$ mm; Right – $h_{talpă} = 1,9$ mm.

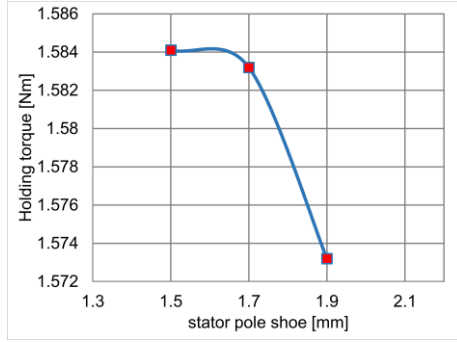


Figure 4.15 Holding torque vs. stator pole shoe.

Increasing the height of the stator pole shoe leads to a local decrease in magnetic flux density. Figure 4.24 shows the magnetic flux density distributions of the transverse magnetic field for three different pole shoe height values (parameter h_{talpa}), namely: 1.5 mm, 1.7 mm, and 1.9 mm. Although the change in the slot cross-section is small, to maintain the same phase resistance, the number of coil turns w_{sp} , had to be adjusted as follows: 237, 235, and 232 turns, respectively.

4.2.8. The influence of the stator yoke height on the holding torque

A final analysis was carried out by modifying the stator yoke height of the motor, as shown in figure 4.28. Since reducing the stator yoke dimension increased the slot area, the number of coil turns was adjusted to maintain the phase resistance value and thus the nominal current.

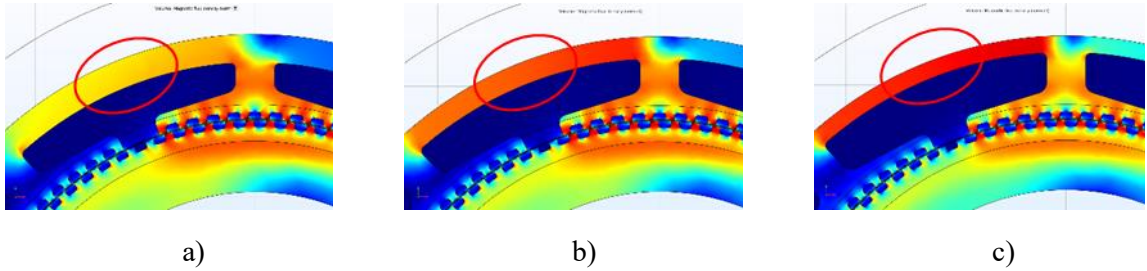


Figure 4.26 Magnetic flux density distribution for three different stator yoke heights:

a) $h_{jug} = 2.5$ mm; b) $h_{jug} = 2$ mm; c) $h_{jug} = 1.5$ mm.

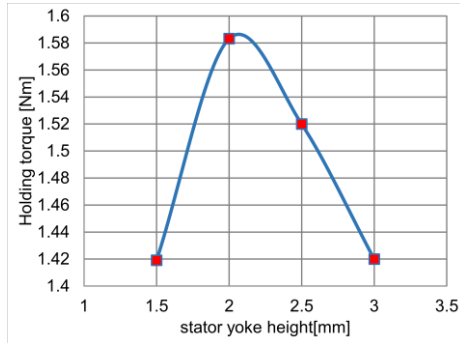


Figure 4.16 Holding torque vs. stator yoke height.

4.2.9. The comparison of the models studied

Table 4.5 shows the numerical results for four models with different permanent magnet heights. Each of these models was optimized to achieve the highest possible holding torque by adjusting the previously mentioned geometric parameters.

Table 4.5 Numerical results obtained for four HSM models.

Model	Number of turns	Cross section area [mm ²]	Height of the permanent magnet [mm]	Cooper volume [cm ³]	Stator inner diameter [mm]	Phase inductance [mH]	Holding torque [Nm]	Electrical time constant [ms]
1	262	92.6	3.5	6.1	52	290	1.38	5.27
2	235	75.7	4.5	4.9	54	190	1.58	3.45
3	203	56.3	5.5	3.6	56	105	1.62	1.9
4	187	47.9	6	3	57	74	1.53	1.34

4.3. HYBRID STEPPER MOTORS WITH MULTIPLE ROTOR STACKS AND DIFFERENT NUMBERS OF STATOR POLES

To increase the torque produced by an HSM while maintaining the mounting flange size and the motor's cross-sectional area, these motors can also be built in multi-stack rotor configurations. To study the influence of the number of rotor stacks on the holding torque developed by the hybrid stepper motor, three numerical models were developed with one, two, and three rotor stacks, respectively. As with the previously studied models, the motor supply conditions (voltage and rated current) as well as the motor's geometric envelope were kept constant.

4.3.1. Influence of the number of rotor stacks on the holding torque

Among the three motors studied, with one, two, and three rotor stacks, the most efficient is the one with two stacks. This is due to its reduced axial length. For motors with greater axial lengths, increasing the number of rotor stacks beyond two may be advantageous. The studied motor has eight stator poles.

4.3.1.1. HSM with one rotor stack (single stack)

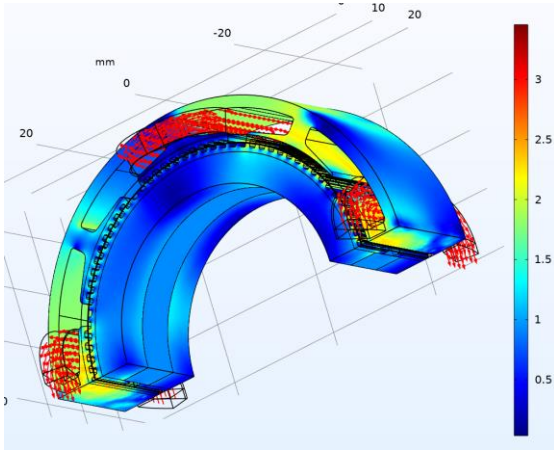


Figure 4.17 Magnetic flux density distribution in the analyzed domain and current density vectors (in red) of the active phase windings.

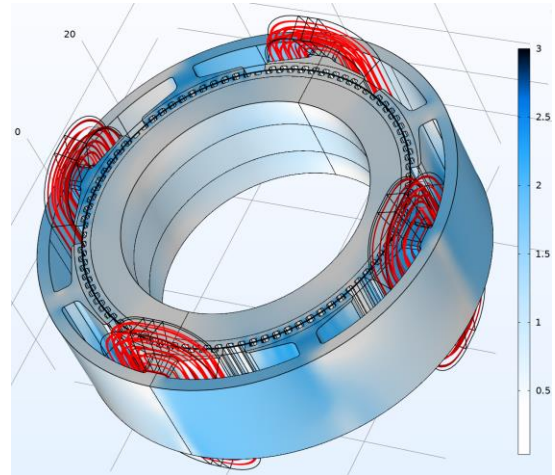


Figure 4.18 HSM with one rotor stack.

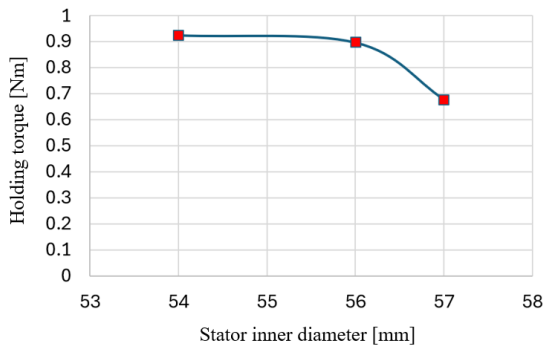


Figure 4.19 Holding torque for HSM with one rotor stack, for different stator diameters.

For this hybrid stepper motor configuration with eight poles and a single rotor stack, several design variants were evaluated. Figure 4.31 shows the variation of the holding torque when the stator winding is supplied with 0,45 A, for different values of the stator diameter (D_{st}), magnet height (h_{mag}), and number of turns (w_{sp}).

4.3.1.3. HSM with three rotor stacks (triple stacks)

This motor was studied using the extended model, as above, detailed in § 4.3.2.

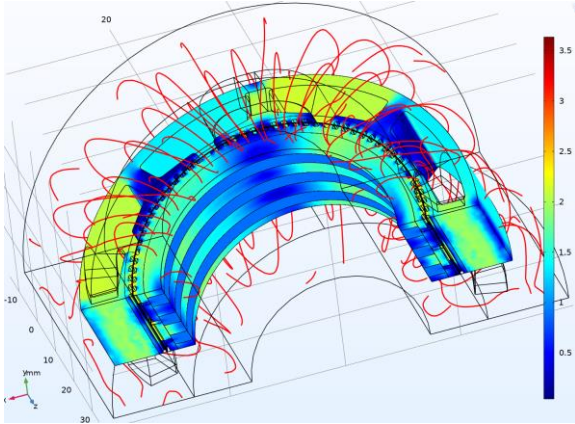


Figure 4.20 Magnetic flux density distribution and the leakage magnetic field lines (in red).

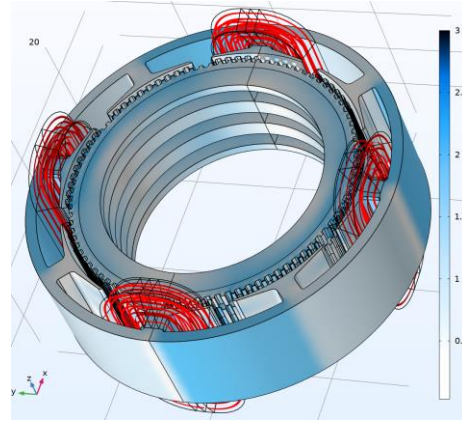


Figure 4.21 HSM with three rotor stacks.

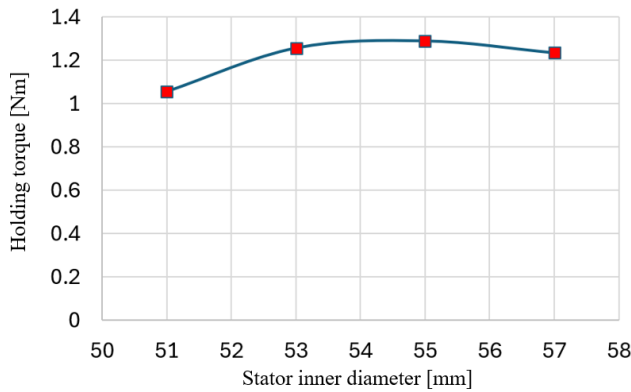


Figure 4.22 Holding torque vs. stator diameter for HSM with three rotor stacks.

The highest torque value of 1.29 Nm was obtained for a magnet height of 5 mm, as shown in figure 4.37. However, this torque is lower than the one obtained for the motor with two rotor stacks, despite the increased number of rotor magnets from two to three.

4.3.2. HSM with different stator poles

As previously shown, the stator poles must be arranged so that the stator teeth are offset by 0° , 90° , 180° , and 270° electrical degrees relative to the rotor teeth. Therefore, in some cases, simply positioning the stator poles according to geometric symmetry is not sufficient. The poles must be shifted from their symmetrical position to ensure the correct alignment of the stator teeth against the rotor teeth, which is essential for proper motor operation.

4.3.2.1. Comparison conditions of the studied design topologies

For this study, in a similar fashion to the previous geometric optimization studies of the hybrid stepper motor, the following parameters were kept constant to ensure consistency when comparing different motor topologies:

- ✓ the axial length of the rotor, the outer and inner diameter of the motor,
- ✓ and the phase current is 0.45A.

4.3.2.2. HSM with 12 poles and two rotor stacks

This model was studied in the two-rotor-stack configuration.

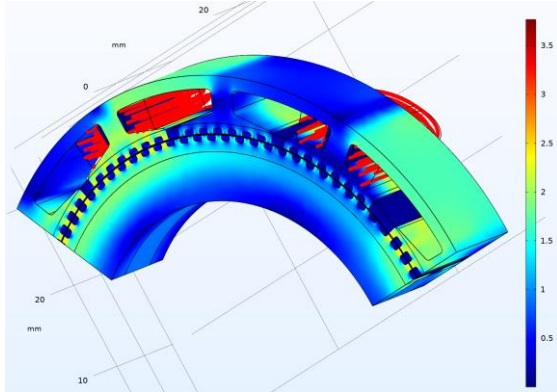


Figure 4.23 Magnetic flux density distribution in the computational domain and current density lines (in red) of the active phase windings.

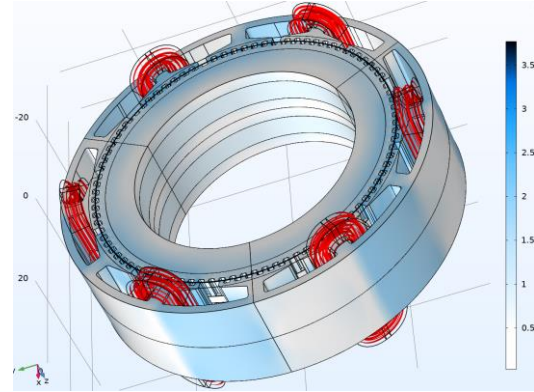


Figure 4.24 HSM with 12 poles and two rotor stacks.

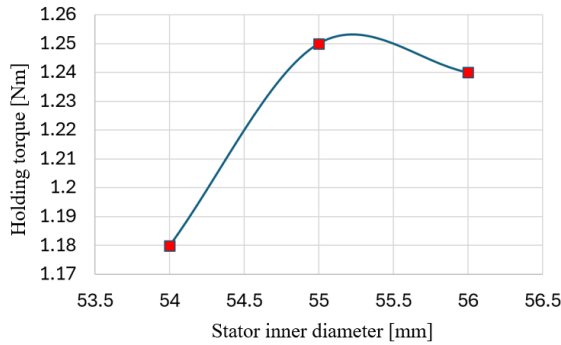


Figure 4.25 Holding torque vs. stator inner diameter for HSM with 12 poles and two rotor stacks.

Figure 4.42 shows the variation of the holding torque as a function of the stator diameter. The highest torque value is obtained for a stator diameter of 55 mm and a permanent magnet height of 5 mm.

4.3.2.3. HSM with 24 poles and one rotor stack

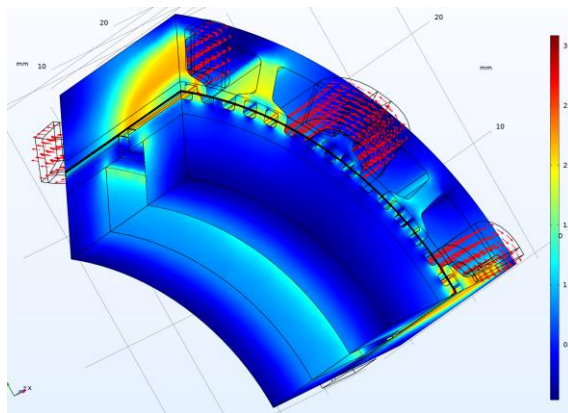


Figure 4.26 Magnetic flux density distribution in the studied domain and current density lines (in red) of the active phase windings.

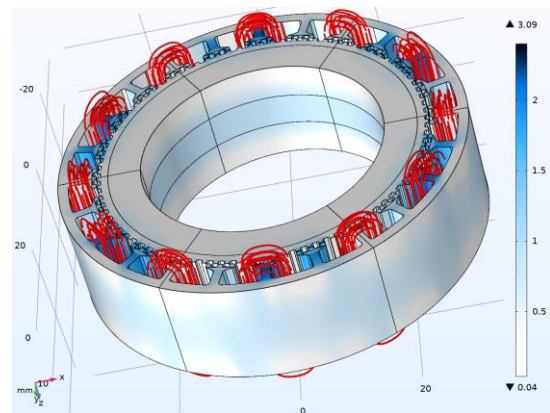


Figure 4.27 HSM with 24 poles and one rotor stack.

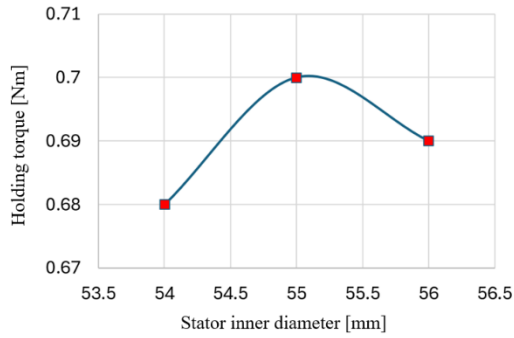


Figure 4.28 Holding torque of the HSM with one rotor stack and 24 poles for different stator diameters.

The bi-phase HSM with 24 poles was studied in a single-rotor-stack configuration. Figure 4.45 shows the variation of the holding torque versus the stator diameter. The highest torque value, 0.7 Nm, was obtained for a stator diameter of 55 mm and a permanent magnet height of 5 mm. This value is noticeably lower than the torque produced by the HSM with a single rotor stack and 12 poles.

4.3.2.4. HSM with 24 poles and two rotor stacks

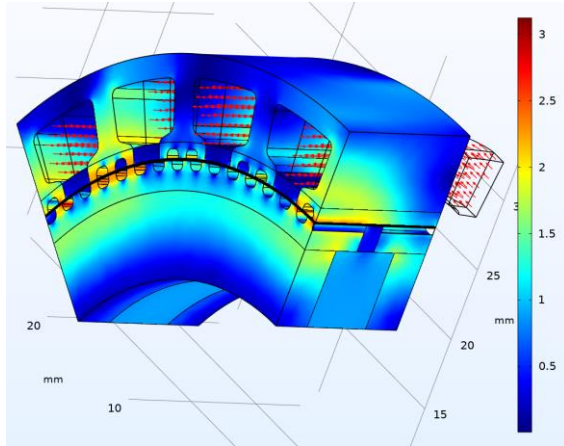


Figure 4.29. Magnetic flux density distribution in the studied domain and current density lines (in red) of the active phase windings.

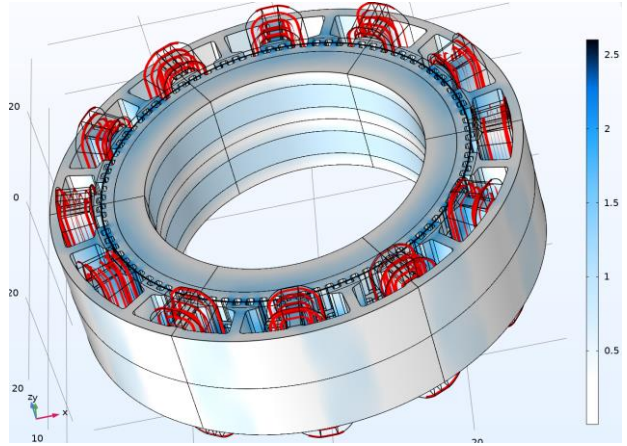


Figure 4.30 HSM with 24 poles and two rotor stacks.

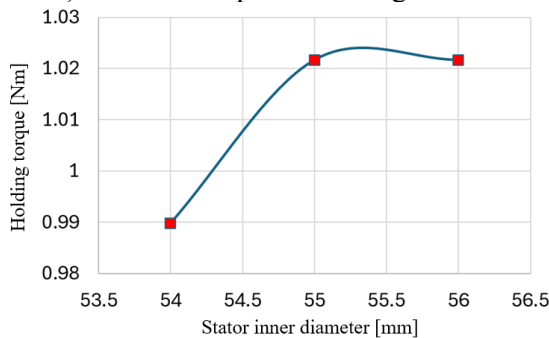


Figure 4.31 Holding torque for HSM with 24 poles and two rotor stacks.

Next, an HSM with 24 poles is analyzed again, but this time in a two-rotor stack configuration. The torque of this motor was higher than that of the HSM with the same number of poles and a single rotor stack, but lower than the torque obtained from the motor with a smaller number of stator poles.

4.3.2.5. HSM with 40 poles and two rotor stacks

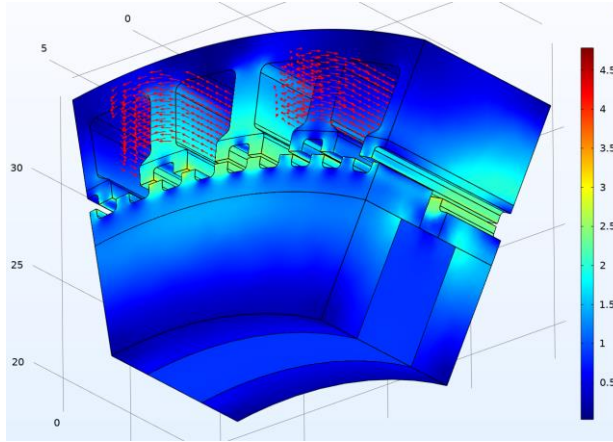


Figure 4.32 Magnetic flux density distribution in the studied domain and current density lines (in red) of the active phase windings.

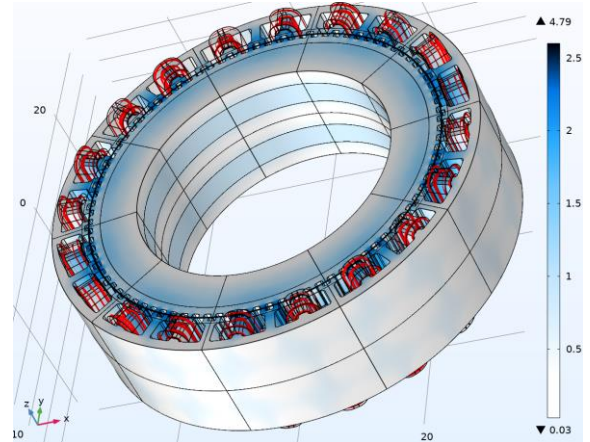


Figure 4.33 HSM with 40 poles and two rotor stacks.

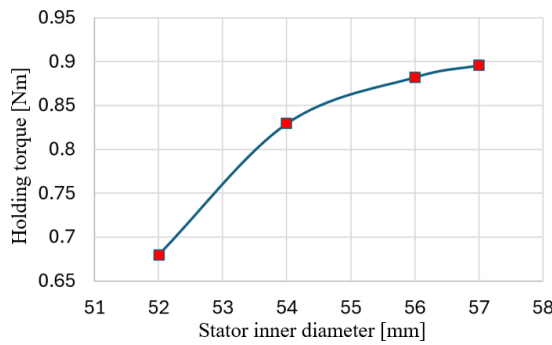


Figure 4.34 Holding torque for different stator inner diameters for HSM with 40 poles and two rotor stacks.

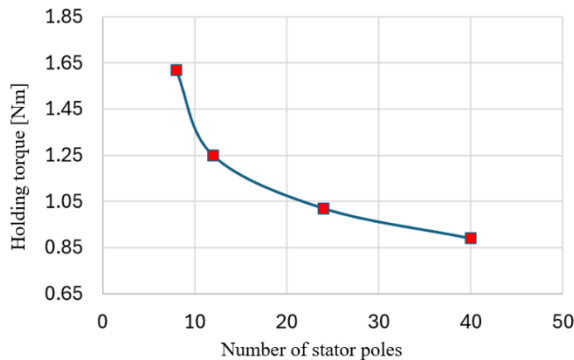


Figure 4.35 Holding torque vs. number of poles for HSM with two rotor stacks.

A comparison of the maximum holding torque obtained for HSMs with different numbers of poles and two rotor stacks is presented in Figure 4.55.

The construction of a hybrid stepper motor with 40 poles, in which the dimensions are fixed and relatively small, as in the case of the studied motor, is not practical due to the very small tooth sizes and the complex winding arrangement. The analysis of this motor is presented below for theoretical purposes, to evaluate the holding torque. For motors with larger diameters and different topologies, designing a motor with a high number of stator poles may be advantageous.

The magnetic flux density distribution and current density vectors in the active coils are shown for the computed domain in Figure 4.52. By replicating the 36° sector ten times and mirroring the geometry along the axial direction, the complete motor geometry and the corresponding flux and current line distributions were obtained, as illustrated in Figure 4.53.

A comparison of the maximum holding torque obtained for HSMs with

5. ANALYSIS OF AN ANISOTROPIC HSM WITH A LAMINATED STATOR AND SOLID ROTOR USING THE EXTENDED MODEL

To analyze the two-phase hybrid stepper motor with a laminated stator and the same nominal parameters as defined in § 4.1, the three-dimensional numerical model described in § 4.2 was used. In addition to the motor data presented in § 4.1, the following key parameters are also specified: permanent magnet height of 3.5 mm, permanent magnet width of 3.5 mm, and 250 turns per coil, corresponding to an inductance of 250 mH.

The extended 3D model was modified to take into account the magnetic anisotropy of the stator. The torque was calculated for the rotor position corresponding to a 90° electrical offset (or 1° mechanical, representing one-quarter of a tooth pitch) between the teeth of the energized stator poles and those of the rotor.

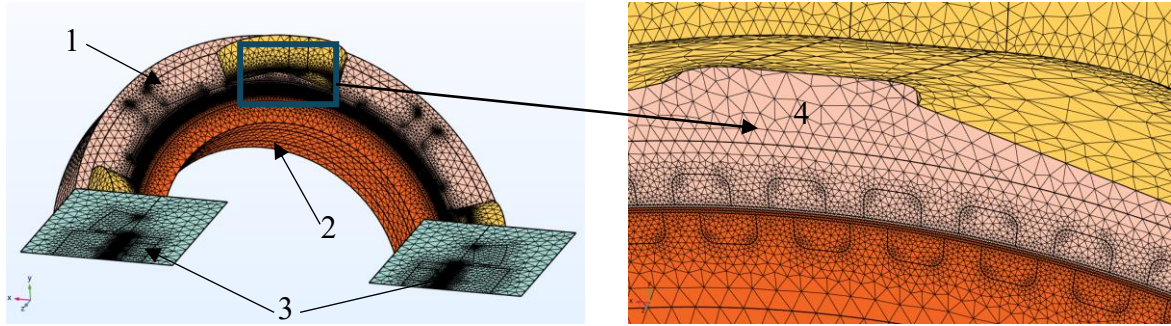


Figure 5.1 3D model of the HSM.

1 - Domains defined with the magnetic vector potential \mathbf{A} , 2 - Domains defined with the magnetic scalar potential V_m , 3 - Periodicity conditions, 4 - Detail of the mesh discretization in the air gap region.

5.1. INFLUENCE OF THE LAMINATION STACKING FACTOR ON THE HOLDING TORQUE

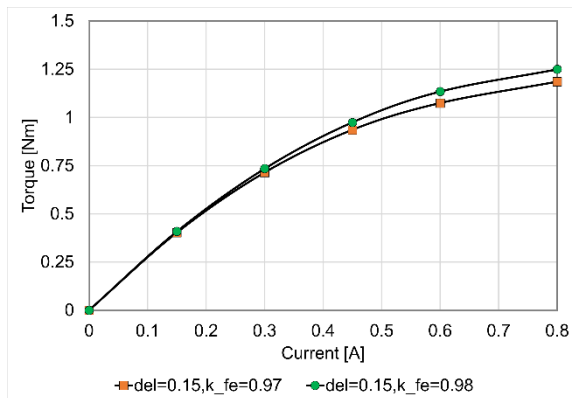


Figure 5.2 Holding torque vs. current for $k_{fe} = 0.97$ și 0.98 .

An initial analysis performed on the motor with an anisotropic magnetic circuit in the stator (stator made of laminated steel) focused on the influence of the lamination stacking factor k_{Fe} on the holding torque. Figure 5.3 shows the variation of the holding torque of the studied HSM as a function of the stator winding current for two slightly different stacking factors: $k_{fe} = 0.97$ and $k_{fe} = 0.98$. As a conclusion, the holding torque of the HSMs can be accurately calculated if the type of lamination and its insulation are known.

5.1. INFLUENCE OF THE AIR GAP HEIGHT ON THE HOLDING TORQUE

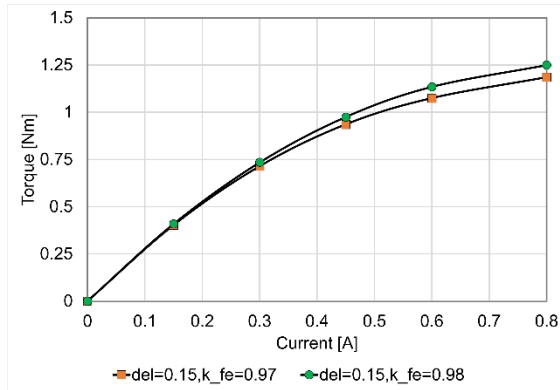


Figure 5.3 Holding torque vs. current for three air gap heights.

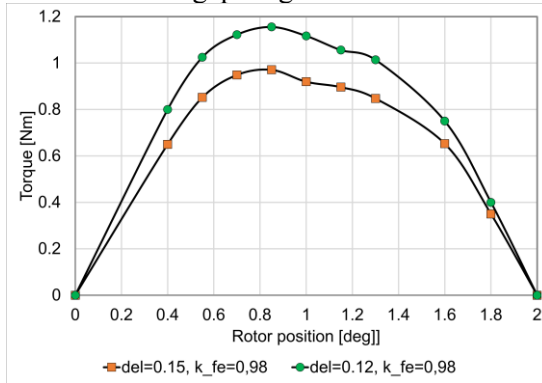


Figure 5.4 Static torque characteristic for two air gap heights and the same stator lamination stacking factor.

5.2. COMPARISON BETWEEN ISOTROPIC (SOLID STATOR) AND ANISOTROPIC (LAMINATED STATOR) MODELS OF THE HSM

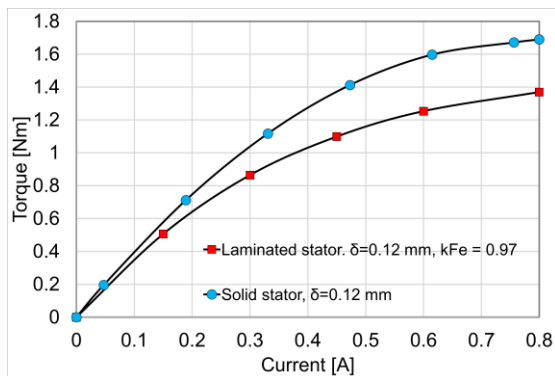


Figure 5.5 Holding torque versus current for the anisotropic (red dots) hybrid stepper motor and the isotropic (blue dots) motor.

torque that is approximately 20% lower around the rated current. This torque reduction is significant and is characteristic of all axial flux motors, such as claw pole motors [4].

Figure 5.5 shows the holding torque versus current curves for three different air gap sizes, with the same stacking factor of the stator laminations.

Figure 5.6 presents the static torque curve for two air gap sizes, while maintaining the same lamination stacking factor, $k_{fe} = 0.98$.

From the analysis of the two curves, it results that a 25% reduction in the air gap size leads to an increase of approximately 20% in the maximum torque. Additionally, the HSM highest torque value (the holding torque) is reached at a rotor displacement angle of around 0.85° , rather than 1° . This significant torque increase while decreasing the air gap was also observed in the motor with a solid stator (the isotropic model) and is characteristic of stepper motors.

The comparison between the torque produced by the HSM with a solid stator, considered isotropic, and that produced by the motor with a laminated stator, considered anisotropic, was carried out using the same geometry and the same materials for both motors.

Due to the non-magnetic insulation between the laminations, the magnetic reluctance along the axial direction of the anisotropic motor is significantly higher than that of the isotropic motor, resulting in a

Figures 5.8 and 5.9 show the magnetic flux density distribution maps for the two types of motors. In the case of the motor with the solid stator, magnetic saturation in the yoke is uniform along the axial direction, from one end of the motor to the other, as shown in Figure 5.11. In contrast, for the motor with the laminated stator, magnetic saturation is non-uniform, as illustrated in Figure 5.10.

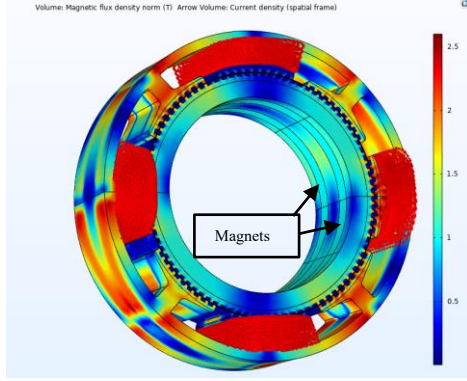


Figure 5.6 Magnetic flux density and current density vectors (red arrows) for the HSM with laminated stator.

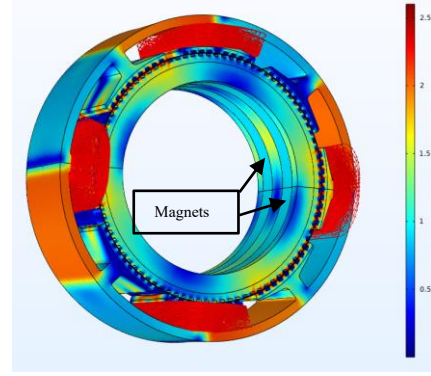


Figure 5.7 Magnetic flux density and current density vectors (red arrows) for the HSM with solid stator.

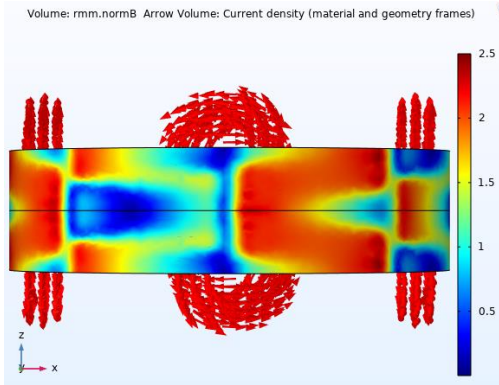


Figure 5.8 Magnetic flux density detail at the yoke level, and current density vector representation (red arrows) for an HSM with a laminated stator.

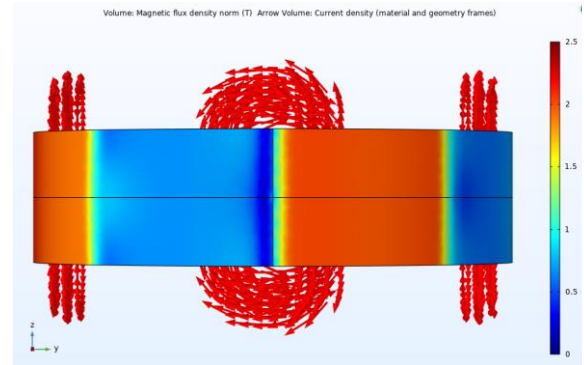


Figure 5.9 Magnetic flux density detail at the yoke level, and current density vector representation (red arrows) for an HSM with a solid stator.

5.3. OPTIMIZATION OF THE HSM WITH LAMINATED STATOR

Following the calibration of the numerical model, taking into account a stator stacking factor of $k_{Fe} = 0.98$ and an airgap of $\delta = 0.15$ mm, conditions for which the numerical results closely match the experimental measurements, the HSM was optimized to produce a higher holding torque.

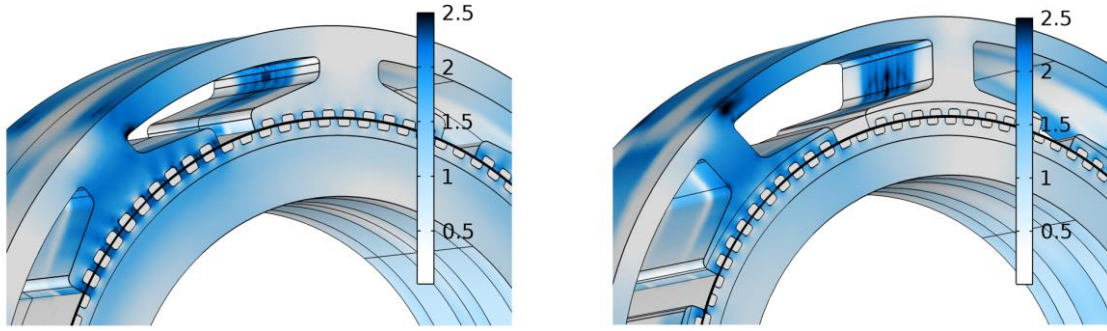


Figure 5.10 HSM with laminated stator: optimized (left) and initial (right).

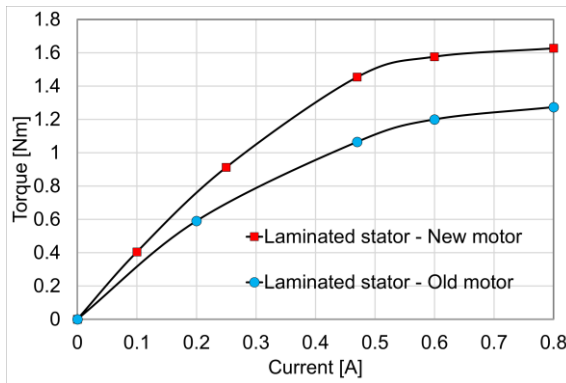


Figure 5.11 Holding torque versus current for the optimized (red dots) and initial (blue dots) HSM.

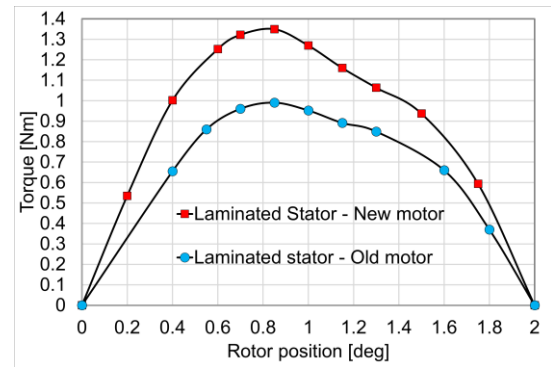


Figure 5.12 Static torque characteristic of the optimized (red dots) and initial (blue dots) HSM.

The optimization of the HSM resulted in a significant increase in holding torque, by approximately 36% at the rated current, while maintaining the same motor envelope, supply current, and stator winding resistance.

6. ANALYSIS OF THE DETENT TORQUE OF THE HSM



Figure 6.1 Division of the air gap into cylinders of equal volume.

For the numerical models used in the study of detent torque, the calculation was performed using Arrkio's method [16]. This method was applied separately for each of the four air gap regions shown in Figure 6.1. Assuming that the variation of the detent torque is approximately sinusoidal, only the maximum detent torque at the zero electrical position was calculated, for simplicity.

6.1. 3D NUMERICAL MODEL OF THE HYBRID STEPPER MOTOR FORMULATED WITH MAGNETIC VECTOR POTENTIAL \mathbf{A}

The first model used for calculating the cogging torque of the HSM was formulated using the magnetic vector potential \mathbf{A} . For this formulation, four torque values were computed, corresponding to four different finite element meshes with varying numbers of elements.

Table 6.1 Computational memory is used for the model defined with the vector potential \mathbf{A} .

Number of unknowns	Memory used	Computation time
11.4 mil	58.31 GB	5 hours 15 minutes
21.6 mil	65.42 GB	6 hours 10 minutes
41.5 mil	93.57 GB	8 hours 13 minutes
68.3 mil	122.7 GB	18 hours 8 minutes

The detent torque calculated for each of the four air gap regions (Figure 6.1), as well as for the entire air gap, is presented in Table 6.2.

Table 6.2 Detent torque calculated for each air gap region.

Number of unknowns	Cylinder 1 [mNm]	Cylinder 2 [mNm]	Cylinder 3 [mNm]	Cylinder 4 [mNm]	Average detent torque [mNm]	Difference between the maximum and minimum value [mNm]
11.4 mil	100.12	102.36	99.92	-	100.8	2.441
21.6 mil	90.53	90.06	88.19	90.0	89.694	2.338
41.5 mil	71.68	71.49	73.63	72.25	72.261	1.95
68.3 mil	63.17	63.35	64.08	64.31	63.729	1.138

6.2. 3D NUMERICAL MODEL OF THE HYBRID STEPPER MOTOR FORMULATED WITH MAGNETIC SCALAR POTENTIAL V_M

Similar to the first model defined using magnetic vector potential \mathbf{A} , four FEM models were developed using the magnetic scalar potential V_m , each with a different mesh discretization.

Table 6.4 presents the computational memory used, the number of unknowns associated with each mesh, and the computation time required to solve the problem. These numerical models were solved using the second PC, with specifications detailed in Table 5.1.

Table 6.3 Memory usage and computation time for solving the model defined with scalar potential V_m .

Number of unknowns	Memory used	Computation time
5.18 mil	17.63 GB	1 hour 6 minutes
6.26 mil	19.59 GB	1 hour 28 minutes
8.65 mil	26.2 GB	1 hour 48 minutes
14 mil	49.08 GB	7 hours 36 minutes

Table 6.4 Detent torque calculated for each air gap region.

Number of unknowns	Cylinder 1 [mNm]	Cylinder 2 [mNm]	Cylinder 3 [mNm]	Cylinder 4 [mNm]	Average detent torque [mNm]	Difference between the maximum and minimum value [mNm]
5.18 mil	47.09	46.73	51.2	-	48.34	4.47
6.26 mil	51.7	53.13	52.16	52,59	52.395	1.43
8.65 mil	54.28	54.33	54.68	54,75	54.51	0.47
14 mil	63.41	63.47	62.14	63,25	63.0675	0.23

6.3. COMPARISON BETWEEN THE NUMERICAL MODEL DEFINED WITH MAGNETIC VECTOR POTENTIAL A AND THAT DEFINED WITH MAGNETIC SCALAR POTENTIAL V_M

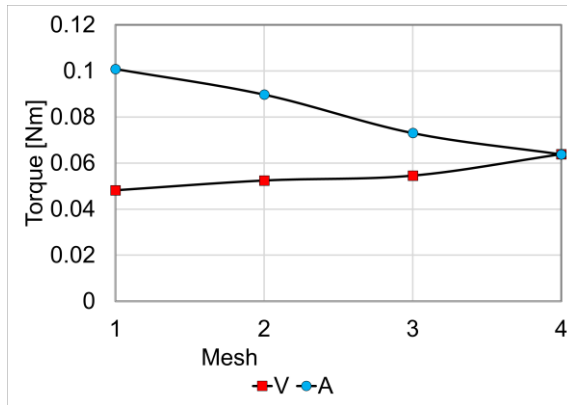


Figure 6.2 Detent torque versus discretization mesh for the two potential-based models.

Figure 6.10 shows the detent torque obtained as a function of the mesh used for the two potential formulations of the studied numerical models (the mesh number increases with the number of finite elements, meaning that mesh 4 is the finest for both potential formulations). From the analysis of the two curves, it can be observed that as the mesh becomes finer, the detent torque calculated for both models converges toward a common value.

6.4. COMPARISON BETWEEN THE DETENT TORQUE OF THE HSM WITH LAMINATED STATOR AND THAT WITH SOLID STATOR

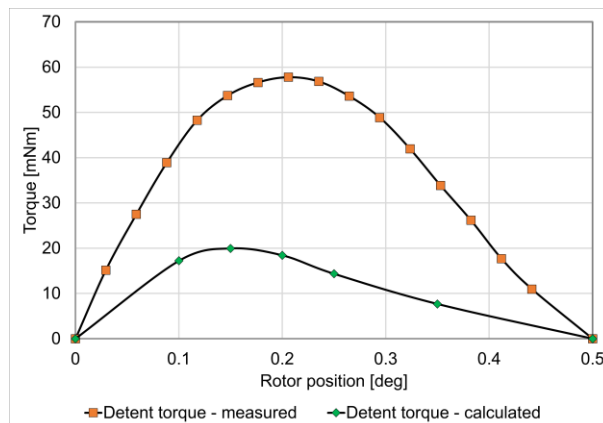


Figure 6.3 Detent torque curve of the non-optimized (orange dots) and optimized numerical model (green dots)

Figure 6.11 presents a comparison of the detent torque for the two studied numerical models. It can be observed that the initial HSM has a maximum detent torque of 20 mNm, while the optimized HSM reaches a detent torque of 70 mNm. In addition, the optimized HSM exhibits a higher holding torque of 1.4 Nm, compared to 1 Nm produced by the initial motor.

7. MANUFACTURING AND TESTING A BI-PHASE HSM PROTOTYPE WITH LAMINATED STATOR

The technological process of manufacturing a two-phase hybrid stepper motor (HSM) involves complex stages, including selecting the ferromagnetic material from the supplier and verifying it, processing the material according to the available technology, applying specific treatments, and assembling the final parts.

The analysis presented in this chapter is based on an HSM prototype developed by ICPE S.A. [80], the MESSICO department, and includes the most important manufacturing processes. In addition, the numerical studies about possible manufacturing deviations are based on this real experimental prototype. However, the calculations presented are relative and indicative, demonstrating the influence of technological processes on the maximum torque produced by the motor.

7.1. HSM PROTOTYPE

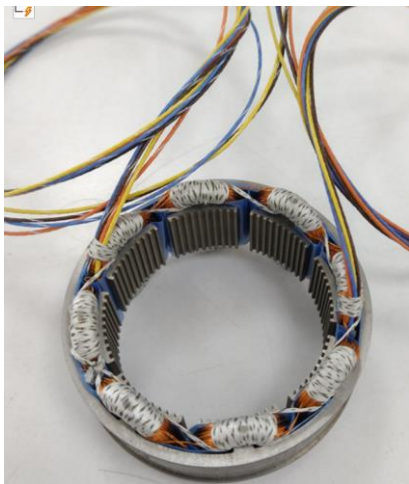


Figure 7.1 HSM stator.

The prototype developed by ICPE S.A. has the technical specifications resulting from the models presented in this thesis, as specified in § 4.1.

For the stator construction, 0.35 mm-thick "Vacoflux" laminations were used (Figure 7.1.a).

The rotor is of the "double stack" type, meaning it has three crowns, each with 90 teeth, incorporating two permanent magnets. The crowns are made of solid "Vacodur" material, and the permanent magnets used are of the Sm_2Co_{17} type (figure 7.6).

Figure 7.8 shows one of the rotor crowns after wire EDM cutting and the assembly consisting of the rotor crowns and permanent magnets after grinding.



Figure 7.2 Left – rotor armature with 90 teeth. Right – Double-stack rotor with permanent magnets.

7.3. VALIDATION OF THE STUDIED TWO-PHASE HSM

7.3.1. Test bench of HSM

The two-phase HSM built according to the specifications in § 7.1 was tested on the test bench shown in Figure 7.14. The bench was designed to allow mounting of the stator in a housing (figure 7.15), installation of the hybrid stepper motor rotor onto the shaft (figure 7.16), and centering of the stator relative to the rotor (figure 7.17), a delicate operation considering that the motor is built without a housing (frameless design) and has a very narrow air gap.

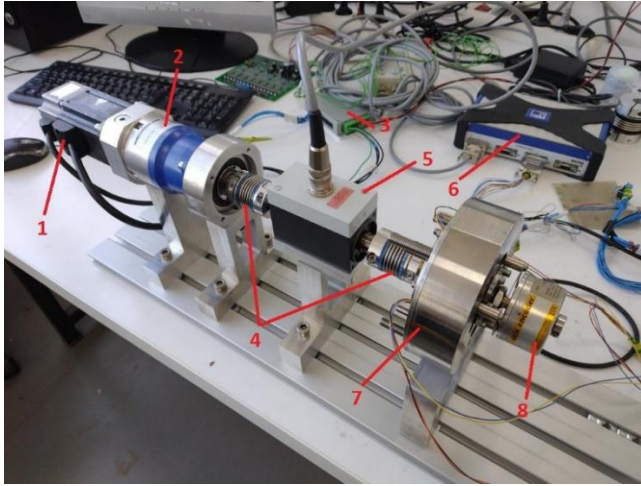


Figure 7.3 The test bench used to measure the HSM torque.

Using this test bench, the static torque characteristics of the HSM were experimentally determined for different stator current values, including the holding torque as a function of current and the detent torque. That allowed the verification of the motor's performance according to the established technical specifications.

7.3.2. Measuring the detent torque

The torque measured with the test bench when the HSM windings are not supplied with currents consists of the following components: *detent torque*, *electromagnetic torque*, *test bench friction torque*, and *parasitic torques*.

7.3.2.1. Measurement of the friction torque

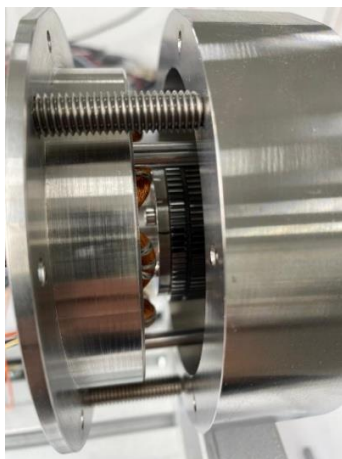


Figure 7.4 Extracting the stator from the motor chase.

To separate the four components of the total torque, firstly was measured torque the friction torque of the test bench. This was done mounting only the rotor on the shaft, while the stator was removed from the housing (Figure 7.18).

To accurately determine the components of the measured torque, the harmonic spectrum of the curve shown in Figure 7.19 was calculated and is presented in Figure 7.21. The period of the measured torque is 360 mechanical degrees, i.e., one full rotation. For this reason, the frequencies are represented in $1/^\circ$.

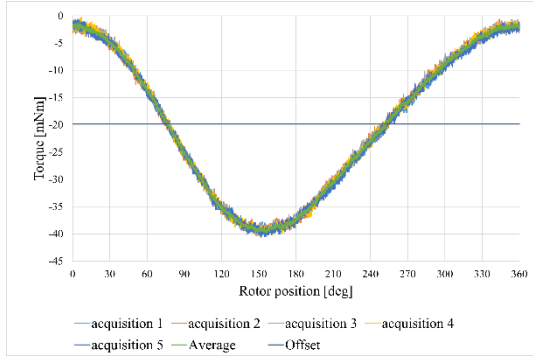


Figure 7.5 Test bench friction torque versus rotor position.

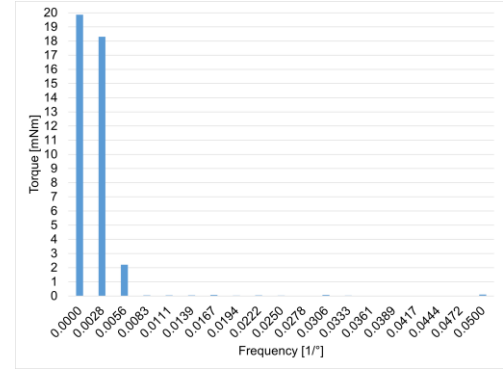


Figure 7.6 Frequency spectral analysis of the test bench friction torque.

7.3.2.2. The measurement of the HSM total torque in the absence of current

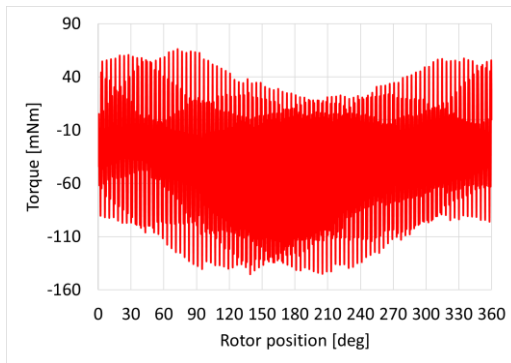


Figure 7.7 Torque variation with rotor position at zero current and 1 rpm.

To determine the torque produced by the HSM, its stator was also mounted, and the rotor was rotated at a constant speed of 1 rpm, in the absence of motor supply. This allowed the measurement of a total torque that includes the friction torque of the test bench, parasitic torques, bending and eccentricity torque, the detent torque of the HSM, and electromagnetic torques due to magnetic hysteresis and eddy currents.

7.3.2.3. Determination of detent torque

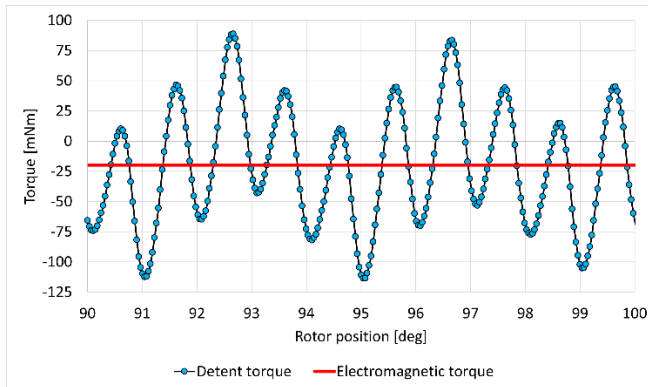


Figure 7.8 Detent torque and magnetic torque vs. rotor position for a 10° rotor movement.

By subtracting the torque curve measured without the stator from the one measured with the stator mounted, the friction torques of the test bench, as well as the bending and misalignment torques, are eliminated. The resulting curve, shown in Figure 7.25, represents the detent torque curve, offset by a baseline (red line) caused by the electromagnetic torque frictional components and any other residual friction between the stator and rotor.

7.3.3. Measuring the HSAM static torque

To measure the holding torque as a function of current, one of the stator phases was supplied with a current in the range of 0.038 A to 0.439 A, and the rotor was rotated using a servomotor with a gearbox at a constant speed of 1 rpm.

Figure 7.27 shows the HSM static torque curve, i.e., the torque versus rotor position curve. From this curve, the friction torque produced by the test bench was subtracted.

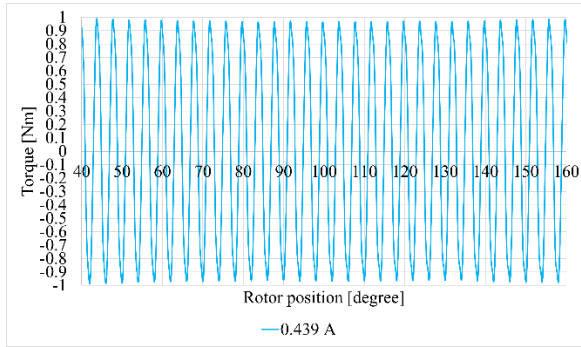


Figure 7.9 Static torque vs. rotor position at 0.439 A current.

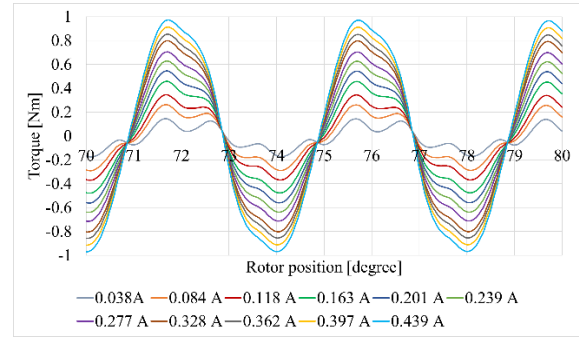


Figure 7.10 Static torque vs. rotor position for currents ranging from 0.038 A to 0.439 A.

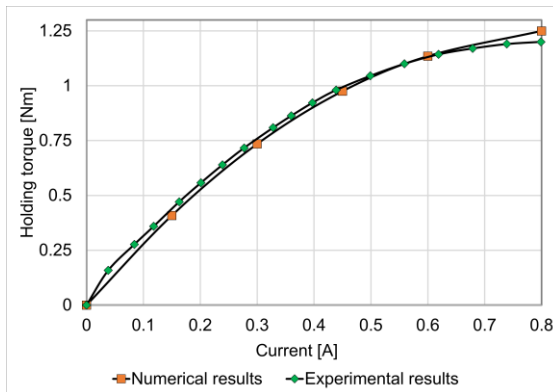


Figure 7.11 Torque vs. current dependence: experimental and numerical.

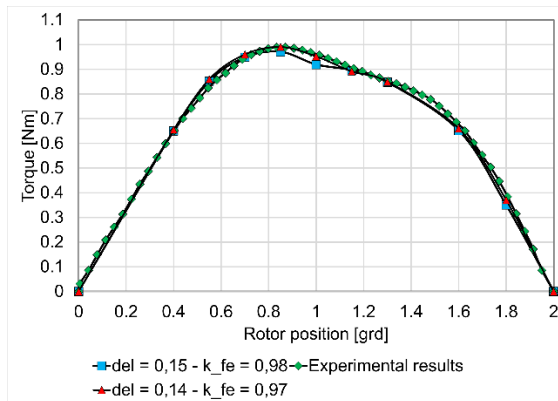


Figure 7.12 Torque vs. rotor position: comparison between numerical and experimental results.

Figure 7.29 shows the experimentally measured holding torque versus current, along with the similar curve obtained from numerical modeling. A stacking factor of 0.98 and an air gap of 0.15 mm were considered in the numerical model.

Figure 7.30 shows the experimentally measured static torque characteristic, compared to the numerically computed curves. The two stacking factors used were 0.97 and 0.98, and the air gap was firstly considered 0.15 mm and then 0.14 mm. As shown in the figure, the static torque characteristics obtained from numerical modeling match very closely the experimentally determined curve, with a maximum error of 2% occurring at a rotor angle of 0.85°.

7.3.4. Comparison between numerical and experimental results

7.3.4.1. Detent torque

Figure 7.31 presents a comparison between the measured detent torque and the torque dependency numerically determined for the non-optimized version of the HSM. The computed curve was obtained using the model based on the magnetic scalar potential V_m formulation and having the finest discretization mesh. The differences between the two curves are significant. They can be explained mainly by the fact that the detent torque is very small, falling under the numerical accuracy of the model, or due to measurement errors.

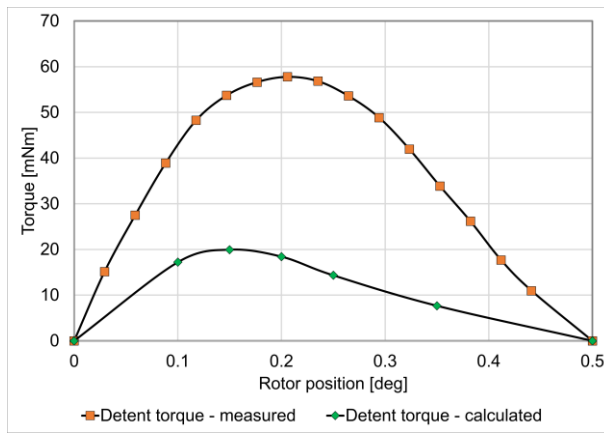


Figure 7.13 Detent torque of the HSM, measured and calculated.

While valid in terms of the shape of the waveform and the harmonic content (including the frequency of the fundamental), the measured detent torque could be affected by the measuring uncertainty of the torque transducer, which has a declared accuracy of 1%, which is ± 0.04 Nm.

7.3.4.2. Holding torque

The measured holding torque is close to the calculated one. Additionally, the static torque curve (figure 7.30), obtained for the rated current, a lamination stacking factor of 0.97, and an air gap of 0.14 mm, matches closely the measured curve, with differences under 5%. The experimental results confirm that numerical modeling can be very accurate, with most of the errors caused by uncertainties regarding the motor exact dimensions obtained through manufacturing process or by differences between real material properties and the one implemented in the numerical models.

8. FINAL REMARKS

As stated in § 1.1, *scope of the thesis*, the author aimed at studying one of the most complex electric motors, the two-phase HSM. The complexity of the motor's geometry, with 90 teeth on each rotor armature, the very narrow air gap, taking into account the stator's active phase end windings, and in the absence of the motor's axial physical symmetry, makes the numerical model particularly challenging.

8.1 RESULTS ACHIEVED

The author aimed to analyze various types of hybrid stepper motors, starting with a model that has specific construction characteristics. The results obtained include conclusions and personal observations related to the complex analysis conducted through numerical modeling of this type of motor. Many of these findings can also be applied to the study of other electric

motors by modeling the magnetic field within complex three-dimensional domains. A brief overview of the results of this work is presented below.

To analyze the efficiency of numerical models utilizing combined vector and scalar magnetic potentials, a model of an HSM with 300 teeth in the rotor and 48 slots in the stator was developed. This motor is special due to its stepping angle of only 0.3° , which is significantly smaller than the 1.8° stepping angle typically found in commercial solutions. The numerical study demonstrates various options for combining the subdomains defined by the two magnetic potentials, many of which may reduce computational effort.

Having the right calculation tools at hand, the most efficient iterative solvers used for FEM modeling were analyzed. Aiming at reducing the computational time to a minimum, 35 combinations of the solvers and preconditioning algorithms were analyzed for solving linear and nonlinear large systems.

Once the most appropriate solving algorithm and the optimal combination of the scalar and vectorial formulations have been identified, a FEM three-dimensional modeling analysis of a two-phase HSM with 90 teeth in the rotor was conducted. Three different models were developed. The first one is a simplified three-dimensional model, neglecting the leakage magnetic flux. The second is an extended model, which takes into account the leakage magnetic flux and the geometry of the end windings. Lastly, the third model was obtained by modifying the second model to consider the magnetic anisotropy of the laminated stator.

To optimize the studied HSM, 24 different geometries were created by varying the geometric parameters and adjusting the number of poles from 8 to 40, using one, two, or three rotor packages. Each of these models required a separate reconstruction of the geometry and an independent calculation of the numerical models.

To accurately measure the extremely low detent torque of a HSM, which is typically only a few tens of milli-newtons, the author develops several high-resolution numerical models. One such model, which is based on the magnetic vector potential formulation, includes an impressive 68.3 million unknowns.

The accuracy of the numerical modeling of the HSM was validated by producing and testing a prototype motor with 90 teeth in the rotor and a stator made from laminations. Experimental measurements indicate that the numerical results are highly accurate, with errors around 3%, which is considered exceptional.

Through numerical modeling, the author managed to optimize the motor, which produced a 30% increase in holding torque compared to the experimental prototype.

8.2 AUTHOR'S ORIGINAL CONTRIBUTIONS

Starting from a real two-phase hybrid stepper motor, with specified nominal parameters, the author developed no fewer than 80 three-dimensional numerical models of stepper motors, many of which have a topology completely different from the initial design. The complexity of the geometry, as well as the large number of resulting unknowns, made this study particularly challenging in terms of modeling, requiring hundreds of hours of computation.

To investigate the most efficient methods for reducing the computation time and memory required to solve 3D models with millions of unknowns, the author conducted a study on combining magnetic vector and scalar potentials in a model of a hybrid stepper motor with 300 rotor teeth. The computational domain was divided in an original manner between the subdomains governed by the two potentials, in a way that differs from the recommendations and formulations found in similar specialized works.

In § 3.5, the author presents no fewer than 35 *cases that apply various iterative solution methods with different preconditioners for solving linear and nonlinear systems of equations*. As a result, a linear system with 40.32 million unknowns was solved in just 1 hour and 18 minutes, and a nonlinear system with approximately 9.65 million unknowns was solved in 50 minutes and 59 seconds. Similar analyses in the literature have typically addressed fewer numerical methods and/or problems with significantly fewer unknowns [5, 7, 8, 52].

Unlike recent articles that focus mainly on optimizing tooth geometry in hybrid stepper motors [10–15, 75–77, 79], the author addresses a much broader range of optimization criteria. In addition to analyzing tooth dimensions, the study also examines tooth pitch, rotor permanent magnet size, air gap, stator yoke height, and stator pole width. In § 4.3, the author conducts an original study of an HSM with a washer-type geometry, characterized by a small difference between the outer and inner diameters. Three-dimensional models were developed for motors with one, two, or three rotor stacks and with 8, 12, 24, and 40 poles. *To create HMSs with different numbers of poles, the author proposed an original method for modifying the poles from their symmetry axis so that the stator and rotor teeth are correctly aligned to ensure proper motor operation. This chapter alone includes the study of 24 hybrid stepper motor geometries, each requiring its geometry construction, meshing, and numerical solution.*

Another important aspect of the work is the calculation of the detent torque of the hybrid stepper motor through numerical modeling. Authors of more recent works that use 3D FEM-based modeling for HSMs have not been able to obtain conclusive results for this torque due to its very low values [9]. In this work, *the author manages to achieve relevant results using high-sensitivity models, calculating a detent torque as low as 20 mNm*. No similar results were found in the reviewed literature.

The thesis also proposes a spectral analysis of the torque variation measured on the test bench, along with a more in-depth interpretation of the results compared to the one provided by the manufacturer.

It is also important to mention that the numerical modeling of the two-phase HSM with a laminated stator, the most difficult and complex model presented in the thesis, enabled *the calculation of the static torque characteristic with an error below 3% compared to the measured curve*. This confirms the accuracy of the models developed by the author, with a level of precision significantly higher than that reported in similar specialized literature.

The relatively large number of models presented in this doctoral thesis, featuring diverse topologies of a compact two-phase hybrid stepper motor, may serve as a source of inspiration and a useful guide for designers of such motors. In addition, the numerical models developed

and the computational techniques used in this work offer practical solutions for solving large-scale matrix systems arising from complex 3D FEM simulations.

8.3 PUBLISHED PAPERS

During the doctoral studies (2021–2025), the following publications in the field of specialization were published:

[1] **Teodor Ionuț Ichim**, Ovidiu Craiu, „*Comparison of two bi-phase hybrid stepper motors, one with solid and the other with laminated stator*”, Rev. Roum. Sci. Techn.–Électrotechn. et Énerg 2025 WOS:001511614200005

[2] Craiu Ovidiu, **Ichim Teodor Ionuț**, „*Geometrical optimization of a bi-phase hybrid stepper motor using FEM*”, University Politehnica of Bucharest Scientific Bulletin Series C-Electrical Engineering and Computer Science, Volume87 Issue1 Page 273-288, WOS:001445507200019

[3] **Teodor Ionuț ICHIM**, Ovidiu CRAIU, „*Modelarea, realizarea practică și testarea unui motor pas cu pas hibrid bifazat*”, Dificultăți și perspective, ACTUALITĂȚI ȘI PERSPECTIVE ÎN DOMENIUL MAȘINILOR ELECTRICE Volumul 2024, Numărul1 / SME'XX

[4] **Teodor Ionuț Ichim**, Ovidiu Craiu, Liviu Cristian Popescu, „*Analyzing a three hundred teeth bi-phase hybrid stepper motor with different numbers of pole pairs*”, Rev. Roum. Sci. Techn.–Électrotechn. et Énerg.Vol.68, 3, pp. 283–288, Bucurest, 2023, WOS:001087001200006

[5] Ovidiu Craiu, **Teodor-Ionuț Ichim**, Liviu Popescu, „*3D FEM Model of a Hybrid Stepper Using Scalar-Vector Potential Formulations*, 2023 13th International Symposium on Advanced Topics in Electrical Engineering (ATEE) | 979-8-3503-3193-6/23/\$31.00 ©2023 IEEE | DOI: 10.1109/ATEE58038.2023.10108283.

[6] Ovidiu Craiu, **Teodor-Ionuț Ichim**, Paul-Matei Craiu, „*Analysis of Iterative Solvers used for Computing a 3D FEM Hybrid Stepper Model*”, 2023 13th International Symposium on Advanced Topics in Electrical Engineering (ATEE) | 979-8-3503-3193-6/23/\$31.00 ©2023 IEEE | DOI: 10.1109/ATEE58038.2023.10108283.

[7] Ovidiu Craiu, **Teodor Ionuț Ichim**, Liviu Popescu, „*FEM study of a synchronous motor with different permanent magnet topologies*”, U.P.B. Sci. Bull., Series C, Vol. 85, Iss. 1, 2023, ISSN 2286-3540. WOS:000983211300012.

[8] Ovidiu Craiu, **Teodor Ionuț Ichim**, Leonard Marius Melcescu, Liviu Popescu, „*Optimization of a High Torque Density Small Hybrid Stepper using 3D FEM Model*”, 2022 International Symposium on Power Electronics, Electrical Drives, Automation and Motion (SPEEDAM) | 978-1-6654-8459-6/22/\$31.00©2022IEEE | DOI: 10.1109/SPEEDAM53979.2022.9842105, WOS:001429387900101.

[9] Ovidiu Craiu, **Teodor-Ionuț Ichim**, „*FEM - Analysis of eddy currents in a BLDC stator liner*”, U.P.B. Sci. Bull., Series C, Vol. 84, Iss. 1, 2022 ISSN 2286-3540. WOS:000809277600012.

Papers published before the doctoral studies:

[1] Ovidiu Craiu, **Teodor Ionuț Ichim**, „*FEM - Circuit Model of a BLDC Motor to Study Phase Advance and Dwell Control*”, 2021 12th International Symposium on Advanced Topics in Electrical Engineering (ATEE) | 978-1-6654-1878-2/20/\$31.00 ©2021 IEEE | DOI: 10.1109/ATEE52255.2021.9425320, WOS:000676164800152.

[2] O. Craiu, **T.I. Ichim**, FEM – „*PWM Circuit Model of a BLDC Motor using COMSOL*”, 2020 International Symposium on Fundamentals of Electrical Engineering (ISFEE) | 978-1-7281-9038-9/20/\$31.00 ©2020 IEEE | DOI: 10.1109/ISFEE51261.2020.9756145. WOS:000812321500015.

[3] Ovidiu CRAIU, Leonard MELCESCU, **Teodor Ionuț ICHIM**, „*Dimensionarea unei înfășurări de amortizare cu ajutorul modelării numerice, pentru atenuarea oscilațiilor unui actuator cu unghi limitat*”, Actualități și perspective în domeniul mașinilor electrice SME20, ISSN / ISSN-L: 1843-5912 <https://www.doi.org/10.36801/apme.2020.1.14>.

[4] Ovidiu Craiu, **Teodor Ionuț Ichim**, Leonard Melcescu, „*Aspecte practice privind proiectarea asistată prin modelarea numerică cu ajutorul programului COMSOL a unui motor fără perii de C.C.*”, Actualități și perspective în domeniul mașinilor electrice SME19, ISSN / ISSN-L: 1843-5912 <https://www.doi.org/10.36801/apme.2019.1.9>

8.4 PERSPECTIVES FOR FURTHER DEVELOPMENT

Building on the experience gained during the undergraduate and master's studies, where the author implemented the numerical modeling of a squirrel-cage induction motor using a complex field-circuit model, and later modeled a drive system consisting of an inverter supplying a BLDC motor, analyzing techniques to extend the speed range such as phase advance and dwell control, the author has expressed a strong interest in continuing research in this field.

Coupled with the professional activity as a design engineer at ICPE S.A., MESSICO department, and in collaboration with the PhD advisor, the author continues the in-depth analysis of electric motors through numerical modeling by developing advanced 3D models for the study of two-phase HSMs.

The author intends to further pursue this research direction by integrating the numerical model developed in COMSOL with a drive system model built in MATLAB-Simulink, or by using a field-circuit modeling approach, in order to analyze the dynamic behavior of the HSM. One potential direction for future research is the numerical study of control techniques used in BLDC motors, such as phase advance and dwell control, and their applicability to hybrid stepper motors.

Furthermore, the author aims to deepen expertise in experimental measurement methods for these motors, as well as for electric machines in general, with a particular focus on small-sized motors. The goal is to separate and precisely measure parasitic torques from useful torques, and to investigate the machine's dynamic behavior.

Last but not least, the author intends to pass on the knowledge and experience acquired through doctoral research to students through academic teaching activities. To this end, the author plans to contribute in the near future to the development of test benches for stepper motors or other permanent magnet motors, to be used as educational tools.

9. SELECTED REFERENCES

- [1] M. K. Jenkins, D. Howe, and T. S. Brich, “*An improved design procedure for hybrid stepper motors*” IEEE Trans. Magn., vol. 26, pp. 2535–2537, 1990.
- [2] J. W. Finch, *Design method for torque estimation in stepping and switched reluctance motors*, 1994 The Institution of Electrical Engineers Printed and published by the IEE Savoy Place London WC2R OBL UK.
- [3] Ki-Bong Jang, Seong-Yeop Lim, Tae-Bin Lim, Chang-Sung Jin, Yun-Hyeon Cho, Young-Tae Kim, and Ju Lee, Member, IEEE, “*2-D FE Analysis of Hybrid Stepping Motor Using Virtual Magnetic Barrier*”, IEEE Transaction on magnetics, VOL. 39, NO. 5, SEPTEMBER 2003.
- [4] Samuel Müller, Marina Keller, Alexander Enssle, Anna Lusiewicz, Philipp Präg, David Maier, Julian Fischer, Prof. Dr.-Ing. Nejila Parspour, “*3D-FEM Simulation of a Transverse Flux Machine Respecting Nonlinear and Anisotropic Materials*”, Excerpt from the Proceedings of the 2016 COMSOL Conference in Munich.
- [5] T. Kosaka and N. Matsui, “*Simple nonlinear magnetic analysis for three-phase hybrid stepping motors*”, Proc. IEEE Industrial Applications Conf., vol. 1, pp. 126–131, 2000
- [6] M.R. Harris, A. Hughes, P.J. Lawrenson, “*Static Torque Production in Saturated Doubly Salient Machines*”, Proc. IEE, Vol. 122.
- [7] C. Stuebig and B. Ponick, “*Comparison of Calculation Methods for Hybrid Stepping Motors*”, in IEEE Transactions on Industry Applications, vol. 48, no. 6, pp. 2182-2189, Nov.-Dec. 2012, doi: 10.1109/TIA.2012.2226994.
- [8] Cornelia Stuebig, Bernd Ponick, *Determination of Air Gap Permeances of Hybrid Stepping Motors for Calculation of Motor Behaviour*, Proceedings of the 2008 International Conference on Electrical Machines
- [9] Alexander Oswald, Hans Georg Herzog, “*Investigation of the usability of 2D- and 3D-FEM for a hybrid stepper motor*”, 978-1-4244-4252-2/09/\$25.00 ©2009 IEEE.
- [10] K. R. Rajagopal, B. Singh, and B. P. Singh, “*Optimal Tooth-Geometry for Specific Performance Requirements of a Hybrid Stepper Motor*”, Digital Object Identifier 10.1109/TMAG.2003.816725, 0018-9464/03\$17.00 © 2003 IEEE.
- [12] I. Ionică, M. Modreanu, A. Morega, C. Boboc, “*Influence Analysis of the Geometry and Materials For the Electromagnetic Torque Calculation on a Stepper Motor*”, The 13th International Symposium on Advanced Topics in Electrical Engineering March, 23-25, 2023, Bucharest, Romania, ISBN: 979-8-3503-3193-6/23/\$31.00 ©2023 IEEE.
- [13] I. Ionică, M. Modreanu, A. Morega and C. Boboc, “*Geometry Influence on the Electromagnetic Torque Calculation of a Stepper Motor*” 2021 12th International Symposium on Advanced Topics in Electrical Engineering (ATEE), 2021, pp. 1-7.

[14] Ioana IONICĂ, Mircea MODREANU, Alexandru MOREGA, Cristian BOBOC, „*Numerical Analysis of a Hybrid Stepper Motor for the Electromagnetic Torque Calculation*”, THE 11th International Symposium on Advanced Topics in Electrical Engineering March 28-30, 2019, Bucharest, Romania, 978-1-7281-0101-9/19/\$31.00 ©2019 IEEE.

[15] Ioana IONICĂ, Mircea MODREANU, Alexandru MOREGA, Cristian BOBOC, „*Design and Modeling of a Hybrid Stepper Motor*”, THE 10th International Symposium on Advanced Topics in Electrical Engineering March 23-25, 2017, Bucharest, Romania.

[20] Paul Acarnley, „*Stepping Motors a guide to theory and practice 4th edition*”, IET CONTROL ENGINEERING SERIES 63. Published by The Institution of Engineering and Technology, London, United Kingdom.

[34] Luca Mariolo, Alberto Rubino, Davide Spelta, Lucia Frosini “*Modeling of Hybrid Stepper Motor Finalized to the Optimization of the Holding Torque*” 978-1-7281-7615-4/21/\$31.00 ©2021 IEEE

[35] Ovidiu Craiu, **Teodor Ionuț Ichim**, Leonard Marius MELCESCU, Liviu POPESCU, “*Optimization of a High Torque Density Small Hybrid Stepper using 3D FEM Model*”, Symposium on Power Electronics, Electrical Drives, Automation and Motion (SPEEDAM) 2022.

[51] A. Arkkio, *Analysis of Induction Motors Based on the Numerical Solution of the Magnetic Field and Circuit Equations*, PhD Thesis, Helsinki 1987.

[52] T. Kosaka", C.Pollock*, N. Matsui**, *3 Dimensional finite element analysis of hybrid stepping motors taking inter-lamination gap into account*, 2004 The Institution of Electrical Engineers. Printed and published by the IEE, Michael Faraday House. Six Hills Way. Stevenage. SG1 2AY

[53] Seong Gu Kang, Dennis K. Lieu, “*Torque Analysis of Combined 2D FEM and Lumped Parameter Method for a Hybrid Stepping Motor*”, 0-7803-8987-5/05/\$20.00 ©2005 IEEE

[54] J. W. Finch, *Design method for torque estimation in stepping and switched reluctance motors*, 1994 The Institution of Electrical Engineers Printed and published by the IEE Savoy Place London WC2R 0BL UK

[55] Ovidiu Craiu, **Teodor-Ionuț Ichim**; Liviu Cristian Popescu, „*3D FEM Model of a Hybrid Stepper Using Scalar-Vector Potential Formulations*”, Published in: 2023 13th International Symposium on Advanced Topics in Electrical Engineering (ATEE), DOI: 10.1109/ATEE58038.2023.10108283

[56] **Teodor Ionuț Ichim**, Ovidiu Craiu, Liviu Cristian Popescu, „*Analyzing a three hundred teeth bi-phase hybrid stepper motor with different numbers of pole pairs*”, Rev. Roum. Sci. Techn.–Électrotechn. et Énerg.Vol.68, 3, pp. 283–288, Bucharest, 2023, WOS:001087001200006

[57] Murat Onsal, Yucel Demir, Metin Aydin, M.K. Guven, “*Impact of Airgap on the Performance of 3-Phase Permanent Magnet Hybrid Stepper Motor*”, IECON 2021 - 47th

Annual Conference of the IEEE Industrial Electronics Society | 978-1-6654-3554-3/21/\$31.00
©2021 IEEE | DOI: 10.1109/IECON48115.2021.958926.

[63] S. Duff, A. M. Erisman, and J. K. Reid. *Direct methods for sparse matrices*. Oxford University Press, London, 1986

[64] Grecu Luminița, -note de curs, *METODE ȘI PROGRAME DE CALCUL NUMERIC*, IMST.

[65] Jianping Zhu, Yingying Liu, Wei Zhuang, Wanchun Tang, „Fast thermal analysis of TSV-based 3D-ICs by GMRES with symmetric successive over-relaxation (SSOR) preconditioning”, 2015 IEEE Electrical Design of Advanced Packaging and Systems Symposium (EDAPS).

[66] R. Lister;J.V. Stone, „Error functions, error signals, and conjugate gradient back propagation”, 1995 Fourth International Conference on Artificial Neural Networks

[67] Abal-Kassim Cheik Ahamed;Frédéric Magoulès,” *Iterative Methods for Sparse Linear Systems on Graphics Processing Unit*”, 2012 IEEE 14th International Conference on High Performance Computing and Communication & 2012 IEEE 9th International Conference on Embedded Software and Systems

[74] K. R. Rajagopal, B. Singh and B. P. Singh, "Optimal tooth-geometry for specific performance requirements of a hybrid stepper motor" in IEEE Transactions on Magnetics, vol. 39, no. 5, pp. 3010-3012, Sept. 2003.

[78] <https://www.vacuumschmelze.com/> (13.04.2025)

[80] <https://www.icpe.ro/ro/> (13.04.2025)

[81] Fu, Z.; Liu, Z.; Liu, X. A, „Dual-Redundancy Two-Phase Hybrid Stepping Motor for Satellite Antenna Drive System.” Energies 2022, 15, 1612. <https://doi.org/10.3390/en15051612>

[87] Craiu Ovidiu, **Ichim Teodor Ionuț**, „Geometrical optimization of a bi-phase hybrid stepper motor using FEM”, University Politehnica of Bucharest Scientific Bulletin Series C- Electrical Engineering And Computer Science, Volume87 Issue1 Page 273-288, WOS:001445507200019

[88] Ovidiu Craiu, **Teodor-Ionuț Ichim**, Paul-Matei Craiu, „Analysis of Iterative Solvers used for Computing a 3D FEM Hybrid Stepper Model”, 2023 13th International Symposium on Advanced Topics in Electrical Engineering (ATEE) | 979-8-3503-3193-6/23/\$31.00 ©2023 IEEE | DOI: 10.1109/ATEE58038.2023.10108283.

[89] Ovidiu Craiu, **Teodor Ionuț Ichim**, Liviu Popescu, FEM study of a synchronous motor with different permanent magnet topologies, U.P.B. Sci. Bull., Series C, Vol. 85, Iss. 1, 2023, ISSN 2286-3540. WOS:000983211300012.

[90] Ovidiu CRAIU, **Teodor-Ionuț ICHIM**, *FEM - Analysis of eddy currents in a BLDC stator liner*, U.P.B. Sci. Bull., Series C, Vol. 84, Iss. 1, 2022 ISSN 2286-3540. WOS:000809277600012.

[91] <https://www.comsol.com/> (13.04.2025)